

See discussions, stats, and author profiles for this publication at: <https://www.researchgate.net/publication/231400089>

# Catalysis with palladium deposited on rare earth oxides: Influence of the support on reforming and syngas activity and selectivity

ARTICLE *in* THE JOURNAL OF PHYSICAL CHEMISTRY · JANUARY 1991

Impact Factor: 2.78 · DOI: 10.1021/j100154a050

---

CITATIONS

29

---

READS

18

5 AUTHORS, INCLUDING:



Francois Le Normand

University of Strasbourg

205 PUBLICATIONS 2,424 CITATIONS

SEE PROFILE



A. Kiennemann

University of Strasbourg

247 PUBLICATIONS 6,192 CITATIONS

SEE PROFILE

on doped and undoped poly-3-methylthiophene films have shown that the extraction of electrons from the valence band results in the closing of the band gap, with the extension of the absorption spectrum from the visible to the near infrared region.

Photoelectrochemical measurements show that the photoactivity of ClAlPc after transformation I is about three times larger than that for an untreated ClAlPc. Under 35 mW·cm<sup>-2</sup> of white light illumination, the photocurrent rises from 0.2 to 0.6 mA·cm<sup>-2</sup>, even if the organic phase becomes disorganized with the introduction of I<sub>3</sub><sup>-</sup> in the film. It is usually admitted<sup>5,42,43</sup> that an increase of crystallinity improves the photoelectronic properties of organic thin films. It therefore means that the negative effect due to the amorphization of ClAlPc upon iodine uptake is largely compensated by the formation of a charge-transfer complex. The photoactivity improvement does not seem to be related to an increase of the film conductivity upon iodine uptake. The series resistances of the film before and after transformation I have been deduced from measurements on the forward region of the dark J-V curves and shown to be comparable. However, the same measurements indicate an increase of the exchange current density,  $J_0$ , from 3 to 13  $\mu\text{A cm}^{-2}$  upon transformation.<sup>11</sup> It seems therefore that the charge-transfer complex between the ClAlPc and I<sub>3</sub><sup>-</sup> generates favorable conditions at the surface of the film for the transfer of

the carriers through the solid-liquid interface. This might occur through the interaction between I<sub>3</sub><sup>-</sup> engaged in the complex and the redox couple (I<sub>3</sub><sup>-</sup>/I<sup>-</sup>) in the solution.

Recent results have shown that there are other routes, besides the formation of a charge-transfer complex, to improve the photoactivity of ClAlPc. Indeed, photocurrents as high as 1 mA·cm<sup>-2</sup> (in the same illumination conditions) have been obtained by transformation of ClAlPc at pH = 3.0 in the presence of 0.1 M Cl<sup>-</sup> or Br<sup>-</sup> anions. As no charge-transfer complexes are expected in these cases, structural modifications have then to be responsible of the photoactivity increase. These systems are presently under investigation.

### Conclusion

The NEXAFS and UPS characteristics of ClAlPc obtained before and after two kinds of film modifications reveal that a charge-transfer complex is formed between the Pc macrocycle and iodine introduced as I<sub>3</sub><sup>-</sup> in the film. The resulting interactions affect the position in energy of the valence band as well as the unoccupied density of states, which leads to an increase of the photoactivity. On the contrary, the low photocurrent activity observed with transformation H goes along with a slight modification of the electronic characteristic of the Pc film.

The peculiarity of transformation H resides in the switch from a parallel to a perpendicular orientation of the Pc macrocycle on the float glass substrate. This is to our knowledge the first time that such a reorganization process is observed on a thick film. Work has been undertaken to study a possible reversibility of this structural change.

(40) Jugnet, Y.; Tourillon, G.; Tran Minh Duc *Phys. Rev. Lett.* **1986**, *56*, 1862.

(41) Tourillon, G.; Flank, A. M.; Lagarde, P. *J. Phys. Chem.* **1988**, *92*, 4397.

(42) Law, K. Y. *J. Phys. Chem.* **1988**, *92*, 4226.

(43) Hor, A. M.; Loutfy, R. O. *Thin Solid Films* **1983**, *106*, 291.

## Catalysis with Palladium Deposited on Rare Earth Oxides: Influence of the Support on Reforming and Syngas Activity and Selectivity

F. Le Normand,<sup>\*,†</sup> J. Barrault,<sup>‡</sup> R. Breault,<sup>§,⊥</sup> L. Hilaire,<sup>†</sup> and A. Kiennemann<sup>§</sup>

*Laboratoire de Catalyse et de Chimie des Surfaces, URA 423 du CNRS, Université Louis Pasteur, 4, rue Blaise Pascal, 67070 Strasbourg Cedex, France; Laboratoire de Catalyse en Chimie Organique, URA 350 du CNRS, Université de Poitiers, 40 Avenue du Recteur Pineau, 86022 Poitiers Cedex, France; and Laboratoire de Chimie Organique Appliquée, URA 469 du CNRS, EEHEICS, 1, rue Blaise Pascal, 67037 Strasbourg Cedex, France (Received: March 28, 1990; In Final Form: July 6, 1990)*

The influence of the support has been tested on the reactivity of Pd/rare earth oxides catalysts (La<sub>2</sub>O<sub>3</sub>, CeO<sub>2</sub>, Pr<sub>6</sub>O<sub>11</sub>, Nd<sub>2</sub>O<sub>3</sub>, Tb<sub>4</sub>O<sub>7</sub>). According to BET surface area, chemisorption, temperature-programmed reduction (TPR) and oxidation (TPO), X-ray diffraction (XRD) and X-ray photoemission (XPS) characterizations, these catalysts have been classified into three classes according to their ability to create anion vacancies: (i) oxides of the type Re<sub>2</sub>O<sub>3</sub> which are unreducible, (ii) CeO<sub>2</sub> where anion vacancies can be created extrinsically by the reduction process, and (iii) Pr<sub>6</sub>O<sub>11</sub> and Tb<sub>4</sub>O<sub>7</sub> where anion vacancies exist due to the nonstoichiometric nature of these oxides. We emphasize also the role of chlorine, coming from the palladium precursor salt, which reacts with the support to form a stable oxychloride phase surrounding the metallic particle and interacting with it. Concerning the catalytic activity, (i) the active site is purely metallic in methylcyclopentane hydrogenolysis, with small selectivity changes on fluorite oxides as compared to Pd/Al<sub>2</sub>O<sub>3</sub> catalysts due to some electronic interaction with the support, but (ii) the mechanism is found to be partly bifunctional in 3-methylhexane aromatization with a large increase in aromatization on Pr<sub>6</sub>O<sub>11</sub> and Tb<sub>4</sub>O<sub>7</sub> supports, and (iii) in syngas conversion, production of high alcohols occurs at the metal-support interface and is favored by the presence of intrinsic anion vacancies on Pr<sub>6</sub>O<sub>11</sub> and Tb<sub>4</sub>O<sub>7</sub> supports. A correlation is found between the density of anion vacancies on these supports and the chain growth probability deduced from the Anderson-Schulz-Flory plot.

### I. Introduction

The use of rare earths as promoters or supports in catalytic reaction has grown extensively in the past few years, due to interesting properties encountered in automotive pollution control

by catalysis or syngas conversion.<sup>1,2</sup> In catalysis by automotive pollution control, the reducibility of some rare earth oxides (CeO<sub>2</sub>, etc.) has been put forward to explain the increase in performance of rare-earth-modified catalysts.<sup>3</sup> In fact, it seems that the easy

<sup>\*</sup> To whom all correspondence should be addressed.

<sup>†</sup> Université Louis Pasteur.

<sup>‡</sup> Université de Poitiers.

<sup>§</sup> EEHEICS.

<sup>⊥</sup> Present address: ALCAN International Ltd, BP 1250, Boulevard Melton (Ed110), Jonquiére, Quebec, Canada 6754K8.

(1) Taylor, K. C. In *Catalysis, Science and Technology*, Anderson, J. R., Boudart, M., Eds.; Springer Verlag: Berlin, 1984; Vol. 5, p 119.

(2) Peters, A. W.; Kim, G. In *Industrial Applications of Rare Earth Elements*; Gscheidner, K. A. Jr., Ed.; ACS Symposium Series No. 164; American Chemical Society: Washington, DC, 1964; Vol. 7, p 117.

TABLE I: Characterization of the Pd/REO<sub>x</sub> Catalysts

support	Pd, wt %	Cl, wt %	Cl/Pd	BET support, m <sup>2</sup> /g	XRD		particle size, nm, from	
					Pd	support	TEM	XPS
La <sub>2</sub> O <sub>3</sub>	7.7	5.4	2.1	20	Y	LaOCl	10–20	25
CeO <sub>2</sub>	8.9	2.6	0.34	27	N	CeO <sub>2</sub>	nd <sup>a</sup>	8
PrO <sub>x</sub>	7.1	1.0	1.1	30	Y	PrOCl, Pr <sub>6</sub> O <sub>11</sub>	8–15	6
Nd <sub>2</sub> O <sub>3</sub>	8.7	6.4	2.1	37				
TbO <sub>x</sub>	7.8	4.8	1.8	9	Y	TbOCl, Tb <sub>4</sub> O <sub>7</sub>	10–20	18
Al <sub>2</sub> O <sub>3</sub>	7.7	0.9	0.35	165	Y	Al <sub>2</sub> O <sub>3</sub>	6.2	7.2
TiO <sub>2</sub>	10.0	0.3	0.1	65				
ThO <sub>2</sub>	6.2	0.8	0.4	5				

<sup>a</sup> Not determined.

reduction of ceria dispersed on such catalysts is favored by the presence of a transition metal (TM) and increases the oxygen storage capacity of the catalyst.<sup>4</sup> Thus the rare earth oxides can store the oxygen during the oxidative step of the exhaust cycle and remove it during the reductive step, thereby broadening the acceptance window of the air to fuel (A/F) ratio. In syngas conversion, the situation is more complicated as both the reducibility and basicity properties of the rare earth oxides have been invoked. Thus on lanthana or other RE<sub>2</sub>O<sub>3</sub> supports (RE = rare earth), the high selectivity of palladium or rhodium toward methanol synthesis is explained by the easy decomposition of CO on basic sites of the support, in a kind of interaction with the transition-metal particle that needs to be elucidated.<sup>5</sup> Moreover some authors have also reported a high selectivity of TM/CeO<sub>2</sub> catalysts (TM = Pd, Rh, Pt) toward higher alcohols (ethanol, etc.).<sup>5a,6</sup> Generally the explanation of such a selectivity involves the activation of CO on an oxygen vacancy of the rare earth lattice at the interface of the TM and the support, providing a site suitable for a chain growth by further dissociation of CO and H<sub>2</sub> on the TM.

Most of these studies involve the use of lanthana and ceria as promoter or support. Only a few studies have been devoted to higher rare earth oxides.<sup>5b,7</sup> It is the aim of this work to get a further insight into the catalytic properties of palladium deposited on higher rare earth oxides and to compare it with the now well-known Pd/La<sub>2</sub>O<sub>3</sub> and Pd/CeO<sub>2</sub> catalysts. We include in this work oxides which crystallize in the fluorite-type structure (CeO<sub>2</sub>, PrO<sub>x</sub>, TbO<sub>x</sub>, ThO<sub>2</sub>) generally easy to reduce but weakly basic and rare earth oxides of the usual hexagonal (A) structure (La<sub>2</sub>O<sub>3</sub>, Nd<sub>2</sub>O<sub>3</sub>). We include also as a reference Pd/γ-Al<sub>2</sub>O<sub>3</sub> and Pd/TiO<sub>2</sub> catalysts, well-known to give an interaction of a different nature between the transition metal and the support under reducing conditions. These catalysts have been characterized by X-ray diffraction (XRD), transmission electron microscopy (TEM), hydrogen and CO chemisorption, temperature-programmed reduction (TPR) and oxidation (TPO), and X-ray photoemission (XPS). Catalytic properties have been tested in both saturated hydrocarbon conversion (methylcyclopentane (MCP) hydrogenolysis and 3-methylhexane (3-MH) aromatization and isomerization) and syngas conversion. We expect that the hydrocarbon catalytic conversion occurs on a metallic site under our conditions, the role of the support being thus to modify the kinetic parameters. To check this point, a careful examination of the selectivity products and <sup>13</sup>C-labeled experiments have been carried out. The product distributions are then compared with published results obtained under very similar experimental conditions. On the other

hand, in the syngas conversion, the active site could involve the support partly or fully. Thus the comparison between the two catalytic behaviors can give us additional information on the nature of the active sites in both reactions and on the nature of the interaction between the support and the metal.

## II. Experimental Part

1. *Products. (a) Support.* The rare earth (RE) and thorium oxides supports were prepared according to the method of Minachev et al.<sup>8</sup> A solution of rare earth nitrate [RE (or Th) (NO<sub>3</sub>)<sub>3</sub>] (10<sup>-1</sup> N) was precipitated at pH = 9 into hydroxide by a few drops of concentrated ammonium hydroxide. The gel was then washed with distilled water until all nitrate ions were removed, dried for 24 h in an oven at 120 °C, crushed and sieved to under 50 μm, and finally calcined under dry air 6 h at 550 °C to remove the carbonate ions.<sup>9</sup> XRD patterns and the change of color during the calcination showed that the stable form of the rare earth oxide was obtained by this preparation for praseodymium oxide (Pr<sub>6</sub>O<sub>11</sub>, black) and terbium oxide (Tb<sub>4</sub>O<sub>7</sub>, dark brown) whereas no color change occurred for the other rare earth oxides after calcination. Samples were then stored in a desiccator. γ-Al<sub>2</sub>O<sub>3</sub> and TiO<sub>2</sub> (P 25) were supplied by Woelm and Degussa, respectively, and were used without any further treatment. Surface areas determined by the BET method (krypton adsorption) are given in Table I. They varied between 5 and 37 m<sup>2</sup>/g.

(b) *Catalysts.* Catalysts were prepared in the conventional way by impregnation of an aqueous solution of Pd(NH<sub>3</sub>)<sub>4</sub>Cl<sub>2</sub> (10<sup>-1</sup> N) onto the support. The solution was then evaporated by heating at 120 °C, and the samples were dried in an oven for 12 h at 120 °C and finally crushed and sieved down to 50 μm. Unless otherwise stated, they were finally calcined under dry air (400 °C, 4 h) and stored in a desiccator before any use. After catalytic tests, the samples were passivated by slow admission of nitrogen followed by synthetic air and stored before characterization studies.

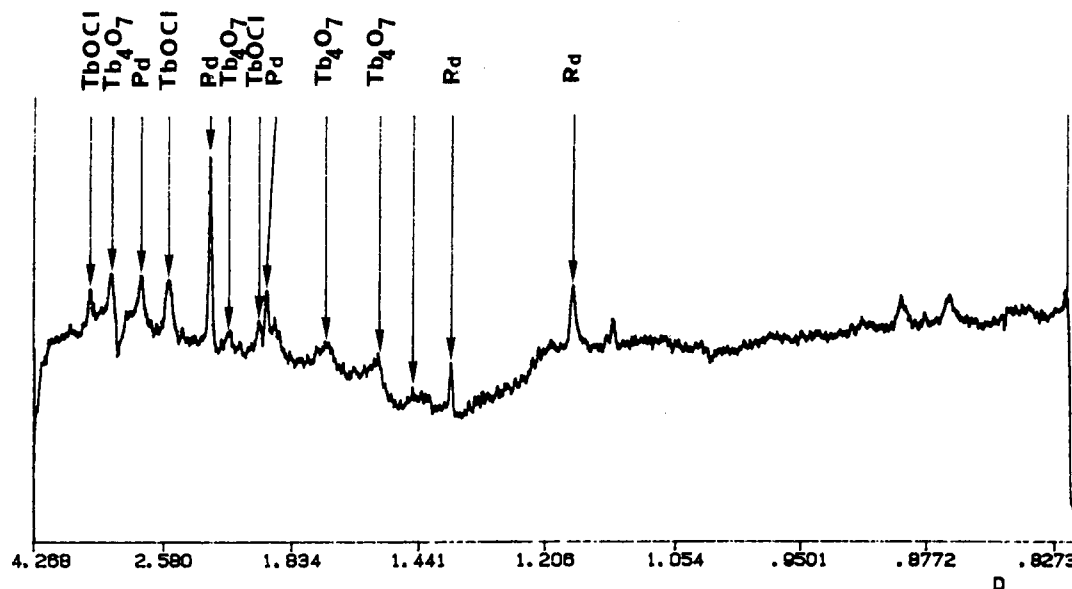
2. *Catalytic Tests. (a) Hydrocarbon Conversion.* The experimental procedure and apparatus have been described elsewhere.<sup>10</sup> The products analysis for MCP hydrogenolysis has also been reported.<sup>11</sup> For 3-MH conversion, the products were analyzed on a capillary silicon OV 101 column. A linear rise in temperature allowed separation of any saturated hydrocarbons between C<sub>1</sub> (methane) and C<sub>7</sub> except for the following:

Methane and ethane: we suppose that the ethane production was negligible compared to the methane production, which is a reasonable assumption for palladium catalysts.

2-Methylhexane (2-MH) and 2,3-dimethylpentane (2,3-DMP) which could only be separated by the gas chromatography-mass spectrometry (GC-MS) coupling device: we suppose that the ratio 2-MH/2,3-DMP determined by GC-MS remained constant whatever the conversion.

Methylcyclohexane (MCH) and *cis*-1,2-dimethylcyclopentane (*c*-1,2-DMCP): as we found a ratio (*t*/*c*-1,2-DMCP) of 4 on

(3) Summers, J. C.; Ausen, A. *J. Catal.* **1979**, *58*, 131.(4) Yao, Y. F. Y. *J. Catal.* **1984**, *87*, 152.(5) (a) Ichikawa, M.; Shikakura, K., *Proceedings of the VIIIth International Congress on Catalysis*; Verlag Chemie: Berlin, 1984; p 925. (b) Vannice, M. A.; Sudhakar, G.; Freeman, M. *J. Catal.* **1987**, *108*, 97. (c) Lee, G. v. d.; Ponec, V. *Catal. Rev.—Sci. Eng.* **1987**, *29*, 183.(6) (a) Diagne, C.; Idriss, M.; Pepin, I.; Hindermann, J. P.; Kiennemann, A. *Appl. Catal.* **1989**, *50*, 43. (b) Katzer, J. R.; Sleight, A. W.; Gajardo, P.; Michel, J. B.; Gleason, E. F.; Macmillan, S. *Faraday Discuss. Chem. Soc.* **1981**, *72*, 121.(7) (a) Mitchell, M. D.; Vannice, M. A. *Ind. Eng. Chem. Fundam.* **1984**, *23*, 88. (b) Rieck, J. S.; Bell, A. T. *J. Catal.* **1986**, *99*, 278.(8) Minachev, Kh.; Khodakov, Yu. S.; Nakhshumov, V. S. *J. Catal.* **1977**, *49*, 207.(9) (a) Fierro, J. L. G.; Mendioroz, S.; Olivan, A. M. *J. Colloid Interface Sci.* **1985**, *107*, 60. (b) Rosynek, M. P. *Catal. Rev.—Sci. Eng.* **1977**, *16*, 111.(10) Corolleur, C.; Corolleur, S.; Gault, F. G. *J. Catal.* **1972**, *24*, 385.(11) Garin, F.; Gault, F. G. *J. Am. Chem. Soc.* **1975**, *97*, 4466.



**Figure 1.** XRD patterns of the Pd/TbO<sub>x</sub> sample, recorded after the calcination, reduction, and hydrocarbon conversion. Lines are assigned from the more intense ASTM files.

Pd/ $\gamma$ -Al<sub>2</sub>O<sub>3</sub>,<sup>12</sup> we supposed this ratio constant to extract the MCH selectivity.

We checked that no diffusional limitations hampered the determination of the activity  $r$  (in  $\mu\text{mol}/(\text{s}\cdot\text{g Pd})$ ) expressed, for a low conversion level  $\alpha_i$ , by

$$r = \alpha_i F / \omega \quad (1)$$

where  $F$  is the hydrocarbon flow ( $\mu\text{mol}/\text{s}$ ) and  $\omega$  is the palladium weight (g Pd). The activity  $r$  was measured after a first pulse of 3  $\mu\text{L}$  of hydrocarbon. No detectable deactivation occurred in the course of the experiment and in the range of temperature considered. The reproducibility in  $r$  determination was about 15%.

In kinetic experiments, the activity  $r$  is defined as

$$r = r_0 \exp(-E_0/RT) \quad (2)$$

where  $E_0$  is the apparent activation energy and  $r_0$  is related to the frequency factor.

The synthesis, purification, and mass spectral analysis of 3-methylhexane-methyl-<sup>13</sup>C have been reported elsewhere.<sup>13</sup>

(b) *Syngas Conversion.* The apparatus for syngas conversion under high pressure has been previously described.<sup>14</sup> The catalysts (about 500 mg) were reduced under hydrogen at 300 °C during 12 h. Then a CO + 2H<sub>2</sub> flow (2 L·h<sup>-1</sup>·g cat<sup>-1</sup>) was admitted through the catalytic bed at  $T = 300$  °C and 100 atm of overall pressure. Products were analyzed after 12 h under flow. Uncondensable products (CO, CO<sub>2</sub>, CH<sub>4</sub>) were analyzed on a condensed Porapak R column. Other products were condensed in water and analyzed on a Chromosorb 101 column.

The CO conversion  $\alpha_s$  is expressed as

$$\alpha_s = \frac{100 \sum N[C_N]}{[\text{CO}]} \quad (3)$$

where  $N$  denotes the number of carbon atoms for the hydrocarbon or alcohol of concentration  $[C_N]$  (in mol/s) produced by the reaction. The selectivity  $S_i$  (%) in the product  $i$  with  $i$  carbon atoms of concentration  $[C_i]$  is defined as

$$S_i = \frac{100i}{\sum N} \frac{[C_i]}{[C_N]} \quad (4)$$

**3. Characterizations of the Catalysts.** (a) *Elemental Microanalysis.* The elemental microanalysis of palladium and

chlorine was performed at the Service Central de Microanalyse du CNRS (Vernaison, France).

(b) *X-ray Diffraction.* X-ray diffraction patterns were recorded on an INEL CPS 120 curved position sensitive detector using the Cu K $\alpha$  line emission selected by a curved quartz monochromator.

(c) *Transmission Electron Microscopy.* TEM was carried out on a Philips EM 400 by depositing the sample on a copper grid coated with carbon. The electron acceleration was 100 keV and the magnification 200 000. The determination of the particles size was difficult due to a poor contrast between the metallic particles and the support. Some microdiffraction patterns have been recorded. The indexation in lattice parameters was calibrated by reference to the gold fcc lattice parameters. On Pd/La<sub>2</sub>O<sub>3</sub> and Pd/PrO<sub>x</sub> we obtained evidence for the oxychloride phase LaOCl and PrOCl. No evidence for such phases (MOCl or MCl<sub>3</sub>) was found on the CeO<sub>2</sub> or  $\gamma$ -Al<sub>2</sub>O<sub>3</sub> supports (Table I).

(d) *Volumetric Characterizations.* H<sub>2</sub> and CO chemisorption, TPR, and TPO were carried out on the same volumetric device described elsewhere.<sup>15</sup>

The following procedure was followed: the dried samples were first reduced in situ up to 400 °C. They were then flushed under an argon stream and cooled to room temperature. Then the hydrogen and CO chemisorption were carried out through the injection of H<sub>2</sub> and CO pulses at 25 °C. The hydrogen pressure on the sample during a pulse did not exceed 30 Torr which prevented the formation of a hydride phase. From the stoichiometry of adsorption, taken in both cases as one, we determined the hydrogen (H/Pd)<sub>C1</sub> and CO (CO/Pd)<sub>C1</sub> rate of chemisorption. Then a temperature-programmed oxidation (TPO) was performed by raising the temperature (4 °C/min) up to 400 °C, followed by an isothermal oxidation at 400 °C. The sample was then flushed under argon at 400 °C (1 h) and cooled to 25 °C, and a temperature-programmed reduction (TPR) was performed up to 400 °C (4 °C/min). The sample was flushed again under argon and cooled to 25 °C. We determined thus the overall oxygen (O/Pd) and hydrogen (H/Pd) consumptions. Finally hydrogen chemisorption was again carried out at 25 °C (H/Pd)<sub>C2</sub>.

(e) *X-ray Photoemission.* Experiments were carried out on a VG ESCA 3 spectrometer equipped with a preparation chamber for thermal treatments under controlled atmosphere. More details on the experimental setup and the analysis procedure are given elsewhere.<sup>16</sup> Energy lines were referred to the C 1s line at 285.0 eV.

(12) Chilles, J. F. Thesis, University of Strasbourg, 1981.

(13) Gault, F. G.; Amir-Ebrahimi, V.; Garin, F.; Parayre, P.; Weisang, F. *Bull. Soc. Chim. Belg.* **1979**, *88*, 475.

(14) Kieffer, R.; Ramarosan, E.; Deluzarche, A.; Trambouze, Y. *React. Kinet. Catal. Lett.* **1981**, *6*, 203.

(15) Guilleminot, A. Thesis, University of Poitiers, 1984.

(16) Le Normand, F.; Hilaire, L.; Kili, K.; Krill, G.; Maire, G. *J. Phys. Chem.* **1988**, *92*, 2561.

**TABLE II: Chemisorption (H<sub>2</sub> and CO), TPR, and TPO on Pd/REO<sub>x</sub> Catalysts**

support	(H/Pd) <sub>C1</sub>	(CO/Pd) <sub>C1</sub>	(O/Pd)	(H/Pd)	ρ <sup>c</sup>	(H/Pd) <sub>C2</sub>
La <sub>2</sub> O <sub>3</sub>	0	0.025	1.10 <sup>a</sup>	2.80	2.55	
CeO <sub>2</sub>	0	0.02	1.50 <sup>a</sup>	3.1 <sup>b</sup>	2.05	0.15
PrO <sub>x</sub>	0	0.01	1.35 <sup>a</sup>	3.70	2.7	
TbO <sub>x</sub>	0	0.01	0.95	2.70	2.8	
Al <sub>2</sub> O <sub>3</sub>	0.18	0.13	1.10	2.90	2.55	0.15

<sup>a</sup> O<sub>2</sub> desorption at 400 °C (very weak in the case of La<sub>2</sub>O<sub>3</sub>- and PrO<sub>x</sub>-supported catalysts). <sup>b</sup> H<sub>2</sub> desorption. <sup>c</sup> ρ = (H/Pd)/(O/Pd).

### III. Results

1. *Characterization Studies.* (a) *Elemental Analysis.* Elemental microanalysis for palladium and chlorine after calcination treatments are reported in Table I. We note generally a high chlorine content with rare earth oxide as support, especially for the case of Re<sub>2</sub>O<sub>3</sub> supports where the Cl/Pd ratio is near 2. On the contrary chlorine was well removed after the catalyst treatment on the Al<sub>2</sub>O<sub>3</sub> and TiO<sub>2</sub> supports. The palladium loading was kept constant at 8 ± 2 wt %.

(b) *X-ray Diffraction.* In Figure 1 we present a typical diffractogram of a Pd/TbO<sub>x</sub> sample calcined and used in hydrocarbon conversion. Besides the patterns of cfc Pd and the stable form of TbO<sub>x</sub> (Tb<sub>4</sub>O<sub>7</sub>), we found patterns that could only be assigned to an oxychloride tetragonal phase TbOCl<sup>17</sup> (patterns at 3.09, 2.78, and 2.534 Å corresponding to the more intense (110), (101), and (111) reflection planes, respectively). We observed the same phase REOCl on the others samples (RE = La, Pr, and Tb), except with CeO<sub>2</sub> support (Table I). We observed also the complete disappearance of the oxide diffraction lines on La<sub>2</sub>O<sub>3</sub>, probably due to a large amorphization of the oxide by reactivity with water which was not completely removed by the low-temperature calcination treatment. Due to the possible occurrence of other phases with praseodymium and terbium oxides, the supports will be named PrO<sub>x</sub> and TbO<sub>x</sub>, respectively, unless otherwise stated.

(c) *TEM.* In spite of the poor contrast between the support and the metallic particles, a visual examination indicates the formation of large particles on La<sub>2</sub>O<sub>3</sub> and PrO<sub>x</sub> supports and smaller particles on CeO<sub>2</sub> support. This is in rough agreement with XRD results as on the latter support only the lines of palladium were not observed. Moreover, the support of the catalyst showed a poor crystallinity due to a high amorphization occurring during the impregnation treatment, in contrast to the high crystallinity of the support alone after a calcination at 550 °C.

(d) *Volumetric Characterizations. Chemisorption.* The results of H<sub>2</sub> and CO chemisorption are given in Table II. As previously described in the Experimental Part, the samples were first reduced under hydrogen at 400 °C and the H<sub>2</sub> and CO chemisorptions were determined before [(H/Pd)<sub>C1</sub> and (CO/Pd)<sub>C1</sub>] and after [(H/Pd)<sub>C2</sub>] the set of TPO-TPR experiments. Before the set of TPO-TPR experiments, we note that the hydrogen chemisorption was zero except on γ-Al<sub>2</sub>O<sub>3</sub>, whatever the nature of the rare earth oxide. However, a small CO chemisorption was observed on all rare earth oxides. After the set of TPO-TPR experiments, the hydrogen chemisorption increased largely on Pd/CeO<sub>2</sub> catalyst. Thus the calcination treatment during the TPO completely changes the chemisorptive properties of the catalysts.

*TPO and TPR.* The stoichiometries of overall oxygen (O/Pd) and hydrogen (H/Pd) consumptions obtained respectively during the TPO and TPR are reported in Table II, whereas the TPO and TPR are represented in Figures 2 and 3, respectively. The oxygen consumptions related to palladium content are expected to be 1 which corresponds to the formation of palladium oxide according to



A higher consumption was obtained with CeO<sub>2</sub> and PrO<sub>x</sub> which could be assigned to some reoxidation of the support such as

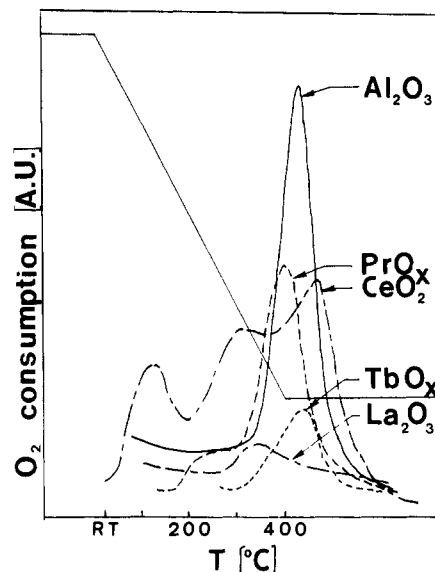
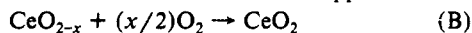


Figure 2. TPO of the Pd-supported catalysts (4 °C/min).

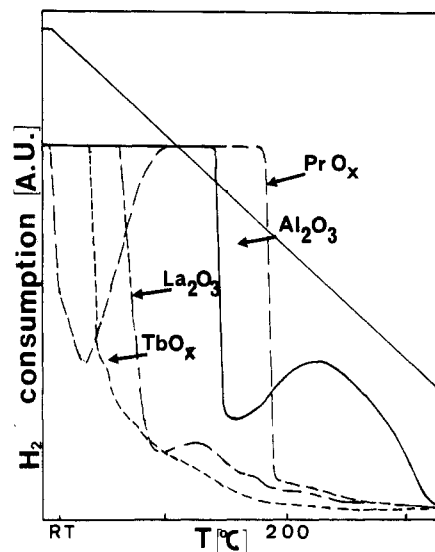


Figure 3. TPR of the Pd-supported catalysts (4 °C/min).

TPO (Figure 2) supports this conclusion, as the main peak of oxygen consumption was observed, whatever the support, between 360 and 400 °C, a range of temperature where the oxidation of palladium is likely to occur,<sup>18</sup> whereas other oxygen consumption takes place at lower temperature in the case of CeO<sub>2</sub> and PrO<sub>x</sub> support. On Pd/CeO<sub>2</sub> catalysts, we note three additional consumptions at around 25, 110, and 260 °C which could be assigned to a reoxidation of the support. Taking into account the work of Yao et al.,<sup>19</sup> the reoxidation of the support CeO<sub>2</sub> may involve three steps which are, in order of decreasing temperature, (i) the filling of oxygen vacancy sites at the interface of the support and the transition metal, then (ii) the filling of surface oxygen vacancy sites of the support, and finally (iii) the filling of bulk oxygen vacancy sites. However, as we obtained some evidence for an easy reoxidation of palladium on CeO<sub>2</sub>,<sup>20a</sup> we could not exclude also some oxygen consumption due to reaction A at temperatures lower than 400 °C. In the same way the oxygen consumption at about 200 °C on Pd/PrO<sub>x</sub> catalyst could be assigned to some reoxidation of the support.

(18) Legare, P.; Hilaire, L.; Maire, G.; Krill, G.; Amamou, A. *Surf. Sci.* **1981**, *107*, 533.

(19) Yao, H. C. C.; Yao, F. Y. Yu. *J. Catal.* **1984**, *86*, 254.

(20) (a) Bernal, S.; Botana, F. J.; Garcia, R.; Kang, Z.; Lopez, M. L.; Pan, M.; Ramirez, F.; Rodriguez-Izquierdo, J. M. *Catal. Today* **1988**, *2*, 653. (b) Le Normand, F.; Barrault, J.; Hilaire, L. *Stud. Surf. Sci. Catal.* **1987**, *30*, 221.

(17) Templeton, D. H.; Dauben, C. H. *J. Am. Chem. Soc.* **1953**, *75*, 6069.

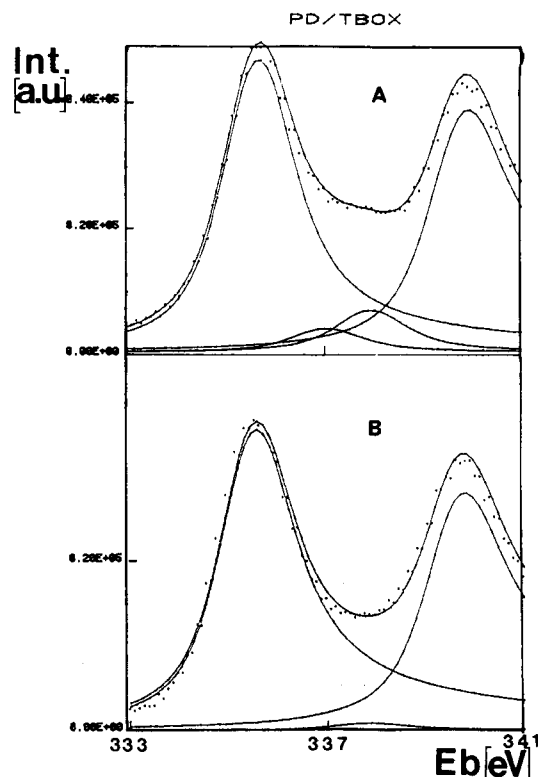
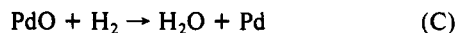
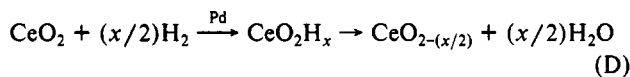


Figure 4. XPS 3d line of palladium on Pd/PrO<sub>x</sub> before and after an in situ reduction (150 °C, 1 atm of H<sub>2</sub>). The fitting procedure has been described in ref 16.

The hydrogen consumptions were always larger than the stoichiometry supposed for the palladium reduction process (Table II):



This implies the occurrence of spillover, a well-known process on transition metal supported on  $\gamma\text{-Al}_2\text{O}_3$ ,<sup>21</sup> or other incorporation of hydrogen on to the support.<sup>22</sup> This process was followed (or not followed) by support reduction according to



Fierro et al. report that dehydration of ceria alone occurs between 300 and 400 °C,<sup>9a</sup> but we can expect that the presence of the transition metal decreases this temperature.<sup>19,20</sup> Such a support reduction may involve, by the creation of oxygen vacancies, the reverse steps already seen in TPO, i.e., the metal-support interface, the surface of the support, and finally the bulk of the support in order of increasing temperature. We can exclude an important hydrogen consumption due to carbonate reduction, as the whole cycle TPO + TPR was repeated and we checked that the hydrogen and oxygen consumptions were reproducible.

Figure 3 clearly indicates that hydrogen was consumed mainly at 25 °C. We must note, however, the singular behavior of Pd/PrO<sub>x</sub> catalyst where additional consumption occurred at higher temperature (110–200 °C). At such temperatures, desorption also occurred, indicating that a dynamic equilibrium between hydrogen adsorption and desorption was established. We must note that the ratio  $\rho$  of hydrogen to oxygen consumption in the TPR and TPO processes was nearly constant at  $2.65 \pm 0.15$  except for Pd/CeO<sub>2</sub> where it was lower. This could indicate that the additional H<sub>2</sub> and O<sub>2</sub> consumptions occurred according to the same process whatever the support and whatever the difference in H<sub>2</sub>

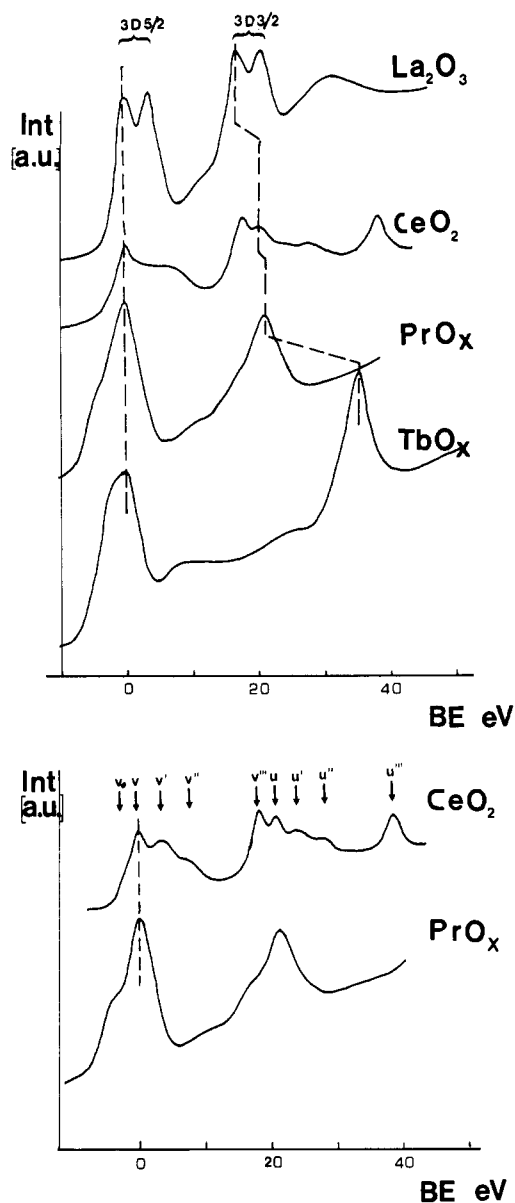


Figure 5. (a, top) TR 3d lines before reduction. The origin of the energy scale is taken at the first well-characterized line. The intensity units are arbitrary. (b, bottom) TR 3d lines after in situ reduction (1 atm of H<sub>2</sub>, 150 °C).

and O<sub>2</sub> consumptions. On the contrary, on Pd/CeO<sub>2</sub> catalysts, the oxygen diffusion seemed to be favored.

In conclusion, we must emphasize the singular behavior of Pd/CeO<sub>2</sub> and, to a lesser extent, of Pd/PrO<sub>x</sub> catalysts. These supports are able to consume H<sub>2</sub> and O<sub>2</sub> at a much higher rate than expected from a simple oxidation–reduction of palladium.

(e) *X-ray Photoemission. Binding Energies.* We present in Table III the binding energies of the main photoemission Pd 3d<sub>5/2</sub> and Cl 2p transitions. They are commonly referred to the C 1s line at 285.0 eV. Most of the samples were reduced before investigation. The influence of a precalcination has been investigated.

Generally palladium was in a metallic state at  $335.1 \pm 0.2$  eV. Before the in situ reduction, a tail was observed on the main metallic peak, revealing the presence of a second line after deconvolutions, at  $3.0 \pm 0.5$  eV toward higher binding energies. This contribution represented between 5 and 20% of the main line (Figure 4A). From similar observations on Pd–Ce/ $\gamma\text{-Al}_2\text{O}_3$  catalysts, we assign this line to a palladium oxychloride species,<sup>16b</sup> the chloride being localized at the interface between the support REO<sub>x</sub> and the metal particle. After in situ reduction, this line disappeared and we obtained a single peak characteristic of metallic palladium (Figure 4B).

(21) Conner, Jr. W. C. In *Hydrogen Effects in Catalysts*; Paal, Z.; Menon, P. G., Eds.; Dekker: Amsterdam, The Netherlands, 1986.

(22) Rojo, J. M.; Sanz, J.; Soria, J. A.; Fierro, J. L. G. *Z. Phys. Chem.* 1987, 149.

**TABLE III: XPS Binding Energies and Surface Ratios of Pd/REO<sub>x</sub> Catalysts (Reference C 1s = 285.0 eV)**

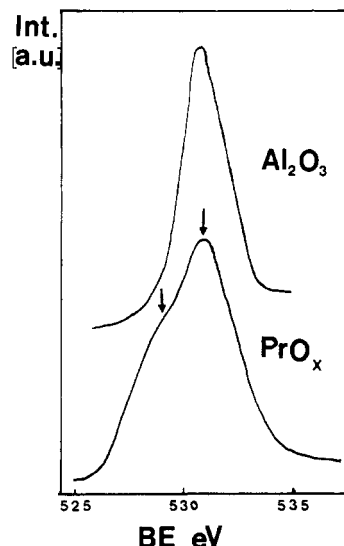
support	calcined <sup>a</sup>	Pd 3d <sub>5/2</sub>	Cl 2p	10 <sup>-2</sup> (Pd/RE)	10 <sup>-2</sup> (Cl/RE)	δ <sup>a</sup>
La <sub>2</sub> O <sub>3</sub>	N	334.9	198.3	5.7	11	136.7
CeO <sub>2</sub>	N	335.6	198.6	9.2	17	137.0
PrO <sub>x</sub>	N	334.9	198.0	15	33	136.9
TbO <sub>x</sub>	N	334.9	198.3	14	19	136.7
Al <sub>2</sub> O <sub>3</sub>	N	335.0	nd <sup>b</sup>	19	nd	nd
CeO <sub>2</sub>	Y	335.1	199.1	12	4	136.0
PrO <sub>x</sub>	Y	335.3	198.3	19	7.7	137.0
Al <sub>2</sub> O <sub>3</sub>	Y	335.5	198.8	12	1.6	136.7

<sup>a</sup> See text for the meaning of δ. <sup>b</sup> Not determined.

The RE 3d lines are represented in Figure 5a for La, Ce, Pr, and Tb, respectively. We note two lines for the light rare earth oxides (La and Pr), apart from the spin-orbit coupling. These spectra are in qualitatively good agreement with previously reported spectra.<sup>23</sup> These two lines are due to a final state effect, the screening of the core hole giving the two final states 4f<sup>n</sup> 3d<sup>9,\*</sup> at higher binding energy and 4f<sup>n+1</sup> 3d<sup>9,\*</sup> at lower binding energy.<sup>24</sup> On the other hand the Ce 3d level gives more complex features whose discussion is beyond the scope of this paper.<sup>25</sup> Briefly the two low binding energy lines are assigned to a mixing of 4f<sup>2</sup> 3d<sup>9,\*</sup> and 4f<sup>1</sup> 3d<sup>9,\*</sup> final states, whereas the high-energy line is assigned to the single 4f<sup>0</sup> 3d<sup>9,\*</sup> final state. Finally the terbium 3d gives one single 4f line with a shoulder which must correspond to a mixing of the 4f<sup>8</sup> 3d<sup>9,\*</sup> and 4f<sup>7</sup> 3d<sup>9,\*</sup> final states. On heavy rare earths, screening effects do not operate as the 4f levels are much too localized and the intensity of these lines can thus directly be related to the initial 4f occupancy.<sup>24</sup>

Reduction of the La, Pr, and Tb cations will result in an increase in the low binding energy contribution 4f<sup>n+1</sup> 3d<sup>9,\*</sup> to the detriment of the high binding energy contribution 4f<sup>n</sup> 3d<sup>9,\*</sup>. The spectra of La<sub>2</sub>O<sub>3</sub>, PrO<sub>x</sub> (Figure 5b), and TbO<sub>x</sub> remained unchanged. On the contrary, on CeO<sub>2</sub>, new lines appeared, noted v<sub>0</sub>, v', and u' on Figure 5b. These lines have been assigned to the final states 4f<sup>2</sup> 3d<sup>9,\*</sup> (v<sub>0</sub>) and 4f<sup>1</sup> 3d<sup>9,\*</sup> (v' and u') for the 5/2 and 3/2 states respectively of an initial Ce<sup>3+</sup> state.<sup>26</sup> Thus photoemission brings strong evidence for a rapid reduction of ceria in the presence of a transition metal as reported elsewhere,<sup>27</sup> a behavior different from any other rare earth oxide used as support. Let us note, however, that surface ceria species are mainly involved in the photoemission process.

Concerning the O 1s line (Figure 6) one single line was obtained at 532.0 eV on γ-Al<sub>2</sub>O<sub>3</sub>, whereas two lines were obtained on rare earth oxides, respectively, at 529.5 ± 0.5 and 531.5 ± 0.5 eV, the intensity of the latter being of the same order of magnitude. We attribute the first line at low binding energy to lattice oxygen, in agreement with the literature.<sup>29</sup> Modification of the oxygen environment by reduction of the oxide of the rare earth cation could not completely explain the shift of 2 eV toward higher binding energies. Recent results, in agreement with the literature, proved that reduction of lattice cation Ce<sup>4+</sup> to Ce<sup>3+</sup> results only in a broadening of the corresponding O 1s line<sup>28,29</sup> due to a very small shift. Thus the second O 1s line could only be explained by hydroxylated or carbonated oxygen surface species that can only be removed by treatment at high temperature. Moreover, careful examination of the C 1s line confirmed the presence of carbonate species, not completely removed by the calcination at 400 °C. This observation points out the higher level of hydroxylation or carbonation of the rare earth oxide surface compared to the alumina surface.

**Figure 6.** XPS O 1s line of Pd/Al<sub>2</sub>O<sub>3</sub> and Pd/PrO<sub>x</sub> catalysts.

**Surface Intensities.** In Table III we note the high value of the molar ratio Cl/support on rare earth oxides, always in large excess relative to the palladium content. The retention of chlorine on cerium promoted or supported catalysts treated at low temperature has already been strongly underlined.<sup>16</sup> The calcination treatment at 400 °C resulted in a large decrease of the Cl/RE ratio on Pd/CeO<sub>2</sub> and, to a lesser extent, on Pd/PrO<sub>x</sub> catalysts, coupled with a small increase of Pd/RE ratio. Moreover, the binding energy difference between palladium and chlorine expressed as

$$\delta = E_b(\text{Pd } 3d_{5/2}) - E_b(\text{Cl } 2p) \quad (5)$$

was constant around 136.8 ± 0.2 eV but decreased by 0.5–1.0 eV on the calcined Pd/CeO<sub>2</sub>. We have noted that δ is indicative of the strength of an interaction between the transition metal and the support through a chlorine bridge.<sup>30</sup> Obviously the nature of this interaction is changed by calcination on Pd/CeO<sub>2</sub>.

In the limit of a low surface area support, the ratio of the intensity of the metallic signal  $I_m$  to the support signal  $I_s$  could be indicative of the palladium dispersion, according to Angevine's formula<sup>31</sup>

$$I_{m/s} = (I_{m/s})_\infty \frac{f[1 - \exp(-c/\lambda_m(E_m))]}{[1 - f(1 - \exp(-c/\lambda_m(E_s)))]} \quad (6)$$

where  $(I_{m/s})_\infty$  represents the ratio of the intensities of m and s, respectively, given by infinitely thick samples,  $\lambda_x(E_y)$  is the mean free path of the electron at the kinetic energy  $E_y$  due to the element x, f is the fraction of support surface covered by the metal, and c is the mean size of a metallic particle. In this formula we neglect the surface coverage by chlorine or other impurities. Assuming for the sake of simplicity that the metallic particles have a cubic shape and  $c/\lambda \gg 1$ , eq 6 reduces to

$$I_{m/s} = (I_{m/s})_\infty \frac{f}{(1 - f)} \quad (7)$$

As

$$f = \frac{ax}{S_{\text{BET}}n_{\text{m}}c} \quad (8)$$

and

$$(I_{m/s})_\infty = \sigma_{\text{m/s}} n_{\text{m/s}} \lambda_{\text{m}}(E_{\text{m}}) / \lambda_{\text{s}}(E_{\text{s}}) \quad (9)$$

where x is the metallic loading,  $n_{\text{m}}$  and  $n_{\text{s}}$  are the density of the metal and support respectively, a is a geometric factor equal to 5 when the particle has cubic shape<sup>32</sup> and  $\sigma_{\text{m/s}}$  denotes the ratio

(23) (a) Jorgensen, C. K.; Berthou, H. *Chem. Phys. Lett.* **1975**, *13*, 186. (b) Sarma, D. D.; Rao, C. N. R. *J. Electron Spectrosc. Relat. Phenom.* **1980**, *20*, 25.

(24) Hillebrecht, V.; Fuggle, J. C. *Phys. Rev. B* **1982**, *25*, 3550.

(25) Kotani, A.; Jo, T.; Parlebas, J. C. *Adv. Phys.* **1988**, *37*, 37.

(26) Le Normand, F.; El Fallah, J.; Hilaire, L.; Legare, P.; Kotani, A.; Parlebas, J. C. *Solid State Commun.* **1989**, *71*.

(27) El Fallah, J.; Hilaire, L.; Le Normand, F. Unpublished results.

(28) Takasu, Y.; Matsui, M.; Tamura, H.; Kawamura, S.; Matsuda, Y.; Toyoshima, I. *J. Catal.* **1981**, *69*, 51.

(29) Barr, T. L. *J. Phys. Chem.* **1978**, *82*, 1801.

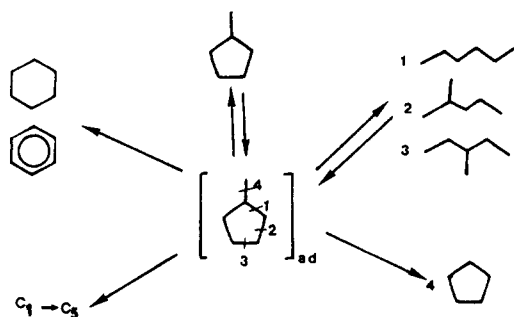
(30) Kili, K. Thesis, University of Strasbourg, France, 1988.

(31) Angevine, P. J.; Vartuli, J. C.; Delgass, W. N. In *Proceedings of the VIth International Congress on Catalysis*; Bond, G. C., Wells, P. B., Tompkins, F. C., Eds.; Londres, 1976; p 611.

**TABLE IV:** MCP Hydrogenolysis on Pd/REO<sub>x</sub> (*T* = 300 °C, *P*<sub>MCP</sub> = 5.2 Torr; *P*<sub>H<sub>2</sub></sub> = 755 Torr)

support	treatment <sup>a</sup>	<i>r</i> , μmol/(s·g Pd)	2-MP	3-MP	<i>n</i> -H	CP
La <sub>2</sub> O <sub>3</sub>	B	0.08	47	31	16.5	5.5
CeO <sub>2</sub>	B	0.20	56	22.5	20.5	1
PrO <sub>x</sub>	B	0.02	54	26.5	16.5	3
Al <sub>2</sub> O <sub>3</sub>	B	0.16	46	26	24.5	3.5
TiO <sub>2</sub>	B	0.92	47	29	19	5
La <sub>2</sub> O <sub>3</sub>	C	0.01	nd <sup>b</sup>	nd	nd	nd
CeO <sub>2</sub>	C	0.04	56	22.5	19	2.5
PrO <sub>x</sub>	C	≤ 3 × 10 <sup>-3</sup>	nd	nd	nd	nd
Nd <sub>2</sub> O <sub>3</sub>	C	0.19	51	27.5	18	3.5
TbO <sub>x</sub>	C	≤ 4 × 10 <sup>-3</sup>	nd	nd	nd	nd
ThO <sub>2</sub>	C	0.03	51	26	16	7
Al <sub>2</sub> O <sub>3</sub>	C	1.14	49	24	19	8
TiO <sub>2</sub>	C	0.44	48	27	22	3

<sup>a</sup>See text for the significance of treatments B and C. <sup>b</sup>Not determined.

**SCHEME I**

of the cross sections for the photoemission line of metal and support respectively as tabulated by Scofield.<sup>33</sup> Assuming that

$$\lambda_m(E_m)/\lambda_s(E_s) \propto (E_m/s)^{1/2} \quad (10)$$

we find finally

$$c = \frac{ax}{S_{\text{BET}}} \left[ \frac{\sigma_{m/s}(E_m/s)^{1/2}}{n_s I_{m/s}} + \frac{1}{n_m} \right] \quad (11)$$

Equation 11 gives an estimation of the mean particle sizes that are reported in Table I. They compare reasonably with the results of hydrogen chemisorption as reported in Table II and thus confirms TEM observations especially on Pd/γ-Al<sub>2</sub>O<sub>3</sub> catalysts. Nevertheless, as some assumptions in the calculation are questionable and as the particle size distribution could be not uniform, this probe can only give us a rough estimation of the mean particle size. This could explain the discrepancy between both methods on Pd/PrO<sub>x</sub> catalyst.

**IV. Catalytic Activity**

**1. Methylcyclopentane Hydrogenolysis.** Let us recall first that all samples were first calcined under dry air at 400 °C.

In Table IV we report the activities (in μmol/(s·g Pd)) for two kinds of reduction, one (B) carried out at 200 °C and the other (C) at 400 °C before the catalytic test, which has been carried out at 300 °C. The products of reaction are depicted on Scheme I.

Blank experiments, performed on ceria support alone, gave negligible activity. We must note first that a direct reduction at 400 °C, without calcination of the samples (treatment A), gave a very low catalytic activity except for Pd/Al<sub>2</sub>O<sub>3</sub> catalyst, in agreement with the reported formation of strong metal-support interaction both on TiO<sub>2</sub> and rare earth oxides.<sup>34</sup>

**TABLE V:** Activation Energies in MCP Hydrogenolysis on Pd/REO<sub>x</sub> ( $\Delta T = 275\text{--}320$  °C, Treatment C)

support	<i>E<sub>A</sub></i> , kcal/mol			
	M2P	M3P	<i>n</i> -H	CP
CeO <sub>2</sub>	60	62	59	67
Nd <sub>2</sub> O <sub>3</sub>	58	62	61	71
TbO <sub>x</sub>	62	63	63	
ThO <sub>2</sub>	53	54	54	
Al <sub>2</sub> O <sub>3</sub>	52	47	47	57

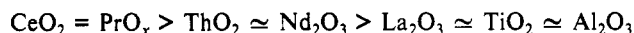
**TABLE VI:** 3-MH Aromatization on Pd/REO<sub>x</sub> (*T* = 360 °C; *P*<sub>3-MH</sub> = 5 Torr; *P*<sub>H<sub>2</sub></sub> = 755 Torr)

support	$\alpha_T$	<i>S<sub>C</sub></i>	<i>S<sub>ID</sub></i>	<i>S<sub>A</sub></i>	<i>r</i>	<i>R<sub>A</sub></i>
La <sub>2</sub> O <sub>3</sub>	4.7	51	37	12	0.81	0.10
CeO <sub>2</sub>	4.0	53	42	5	3.80	0.19
CeO <sub>2</sub> <sup>a</sup>	4.1	66	28 <sup>b</sup>	6	0.4 <sup>c</sup>	2.4 × 10 <sup>-4</sup>
PrO <sub>x</sub>	4.2	38	43	19	2.50	0.57
Nd <sub>2</sub> O <sub>3</sub>	3.1	67	23	10	0.43	0.05
TbO <sub>x</sub>	5.8	71	9	20	0.84	0.24
TiO <sub>2</sub>	7.2	65	32	3	0.45	0.04
Al <sub>2</sub> O <sub>3</sub>	4.0	50	41	9	9.9	0.79

<sup>a</sup>Support alone. <sup>b</sup>Mainly olefins. <sup>c</sup>In μmol/(s·m<sup>2</sup> BET).

After reduction of high temperature, following the calcination (treatment C), the activity was very low for most samples with RE oxides as support, but not on Pd/TiO<sub>2</sub> and Pd/Al<sub>2</sub>O<sub>3</sub> catalysts (Table IV). On comparing the influence of treatments B and C on the catalytic activity, the net result was a decrease, from a factor of only 2 on Pd/TiO<sub>2</sub> to values higher than 5 on Pd/REO<sub>x</sub> catalysts. Thus the nature of the strong metal-support interaction is different on TiO<sub>2</sub> and on the RE oxides support. On the contrary, on Pd/Al<sub>2</sub>O<sub>3</sub> catalyst, the activity increased by almost 10 with a higher reduction temperature.

The selectivities in MCP hydrogenolysis include the direct formation of 2- and 3-methylpentane (2-MP and 3-MP, respectively), *n*-hexane (*n*-H), and cyclopentane (CP) formed by the initial hydrogenolysis of the endo (rupture 1,2,3) or exocyclic (rupture 4) carbon-carbon bond (Scheme I). Extensive cracking or ring enlargement was negligible under our conditions, except on Pd/PrO<sub>x</sub> and Pd/TbO<sub>x</sub> where some cyclohexane formation was detected. Selectivity distributions are reported in Table IV for low conversion rates (≤4%). The reproducibility in 2-MP selectivity, the main product, was ±2%. We did not observe any important change in the product distribution with the reduction temperature. However, small but definite and reproducible changes occurred according to the nature of the rare earth. Then the selectivities in 2-MP ranged from around 55% to 45% according to the sequence



We note that the oxide supports of the fluorite type are the most efficient in 2-MP selectivity.

Activation energies for each carbon-carbon rupture are reported in Table V together with some Arrhenius plots  $\log r_i = f(1/T)$  (Figure 7, a and b). The results show, whatever the carbon-carbon bond rupture, a higher activation energy by about 10 kcal/mol on palladium supported on rare earth oxides or ThO<sub>2</sub>, compared to Pd/γ-Al<sub>2</sub>O<sub>3</sub>. Furthermore, we note on catalysts supported on rare earth oxides a linear correlation between the activation energy and the frequency factor for each carbon-carbon bond rupture. This compensation effect is well-known in catalysis and has received many explanations.<sup>35,36</sup> Moreover, we note that, for Pd/γ-Al<sub>2</sub>O<sub>3</sub>, the compensation curve has a slightly different slope.

**2. 3-MH Aromatization. Overall Results.** In Table VI the total activity *r* and the aromatization activity *r<sub>A</sub>* are reported together with the selectivity in the main products, i.e., hydro-

(32) Boudart, M.; Djega-Mariadassou, G. *Cinétique des réactions en catalyse hétérogène*, Masson: Paris, 1982; p 26.

(33) Scofield, J. H. *J. Electron Spectrosc. Relat. Phenom.* **1976**, *8*, 129.

(34) Meriaudeau, P.; Dutel, J. F.; Dufaux, M.; Naccache, C. *Stud. Surf. Sci. Catal.* **1982**, *7*, 95.

(35) Galwey, A. *Catal. Rev.—Sci. Eng.* **1977**, *26*, 247.

(36) Conner, Jr. W. C. *J. Catal.* **1982**, *78*, 238.



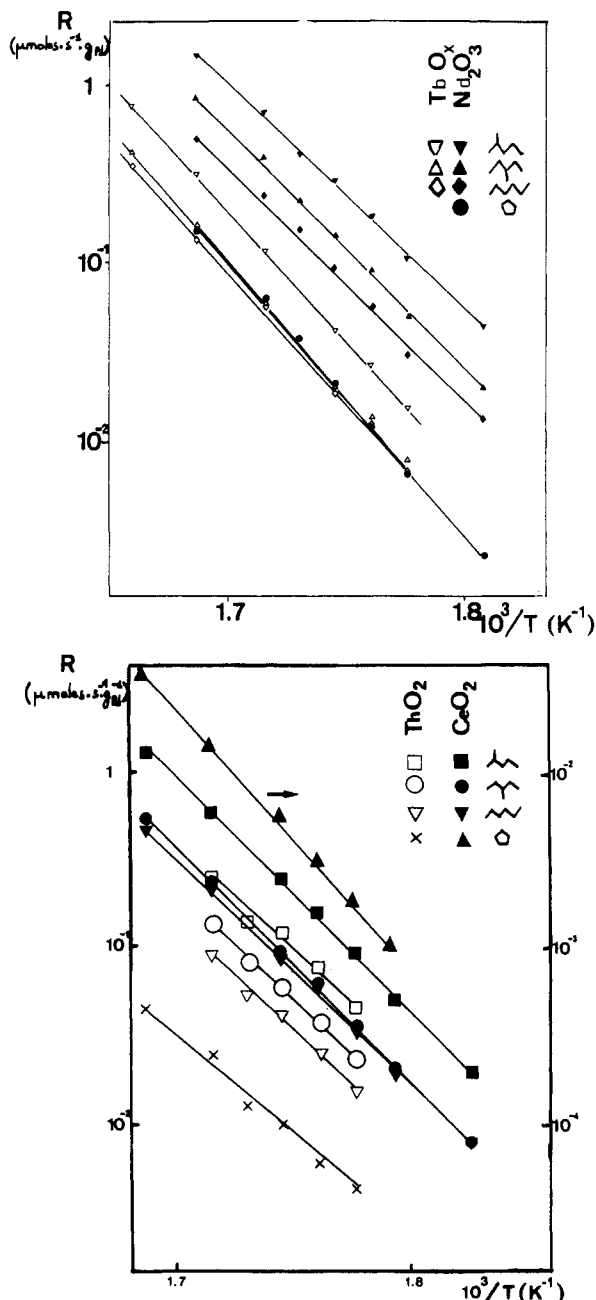
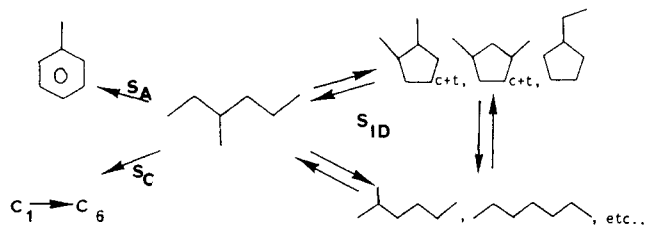


Figure 7. (a, top) Arrhenius plot  $\log R_i = f(1/T)$  on Pd/TbO<sub>x</sub> and Pd/Nd<sub>2</sub>O<sub>3</sub>. (b, bottom) Arrhenius plot  $\log R_i = f(1/T)$  on Pd/CeO<sub>2</sub> and Pd/TbO<sub>2</sub>.

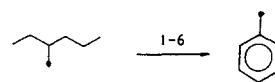
#### SCHEME II



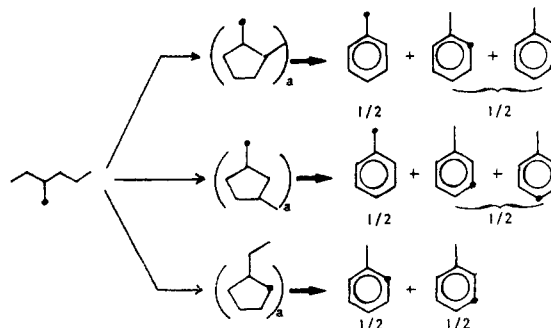
cracking  $S_C$ , isomerization and dehydrocyclization  $S_{ID}$  and aromatization  $S_A$  (Scheme II).

Whereas both isomerization and dehydrocyclization could be considered as reversible processes in our conditions, the hydrocracking and the aromatization are irreversible.<sup>37</sup> Moreover, it is now well-known that isomerization on palladium occurs mainly according to a cyclic mechanism, which makes hopeless any differentiation between dehydrocyclization and isomerization

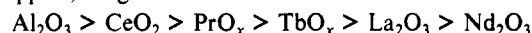
#### SCHEME III



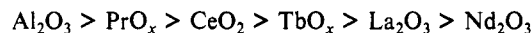
#### SCHEME IV



products.<sup>38</sup> First we must note that the activity of the support alone, contrarily to the MCP hydrogenolysis, was not negligible. The main reactions were hydrocracking according to an internal carbon-carbon bond rupture, dehydrogenation, and aromatization. The total activity on palladium-supported catalysts, according to the support, ranged as follows



while the sequence in aromatization activity  $r_A$  was somewhat different:



These results point out the high aromatization activity on PrO<sub>x</sub>, CeO<sub>2</sub>, and TbO<sub>x</sub> compared to the La<sub>2</sub>O<sub>3</sub> and Nd<sub>2</sub>O<sub>3</sub> supports. Particularly on Pd/PrO<sub>x</sub> and Pd/TbO<sub>x</sub> the results compared fairly well with Pd/Al<sub>2</sub>O<sub>3</sub> catalysts, whereas the dispersion of palladium on the rare earth support was substantially lower. Thus we investigated specifically the aromatization mechanism on Pd/Al<sub>2</sub>O<sub>3</sub> and the Pd/PrO<sub>x</sub> catalysts. Activation energies in aromatization were respectively 56 and 65 kcal/mol determined between 320 and 360 °C but were reduced by a factor of 2 at higher temperatures in both cases, suggesting kinetical limitations by a diffusion process. Nevertheless, the frequency factors were respectively  $2.1 \times 10^{14}$  and  $1.7 \times 10^{11}$  mol/(s.g Pd), indicating a much higher density of specific sites for aromatization on Pd/PrO<sub>x</sub> catalysts.

**Mechanistic Studies Using Labeled 3-MH.** We performed experiments with labeled 3-methylhexane-*methy*-<sup>13</sup>C. The use of such a molecule allows us to separate the direct aromatization mechanism occurring through 1-6-cyclization according to Scheme III and an indirect mechanism obtained by 1-5-cyclization followed by ring enlargement according to the following pathways (Scheme IV). Indeed the demethylation in the source of the mass spectrometer occurs exclusively by rupture of the exocyclic carbon-carbon bond, giving a cyclohexane fragment. We note  $a_6$  the ratio of C13 enrichment for the demethylated fragment relative to the C13 enrichment of the reactant molecule. Thus  $a_6$  gives us directly the contribution of the indirect mechanism.<sup>39</sup>

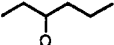



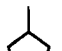
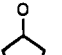
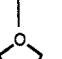
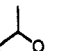
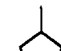
Higher  $a_6$  values are obtained on Pd/PrO<sub>x</sub> as compared to Pd/Al<sub>2</sub>O<sub>3</sub> under the same experimental conditions (Table VIIA). However, we must compare the two catalysts for the same levels of aromatization  $\alpha_A$  and total  $\alpha_T$  conversions, a situation that we found on Pd/ $\gamma$ -Al<sub>2</sub>O<sub>3</sub> by considerably lowering the hydrogen pressure from 760 to 38 Torr.<sup>12</sup> Then the isotopic distributions on the two catalysts compared fairly well, within experimental accuracy. Thus the high selectivity toward aromatization on Pd/PrO<sub>x</sub> is probably due to a strong modification of the surface reaction kinetics parameters, i.e., a decrease in hydrogen and/or an increase in hydrocarbon partial pressure, rather than a change in the reaction mechanism. The main mechanism of aromatization

(38) Hajek, M.; Corolleur, S.; Corolleur, C.; Maire, G.; O'Connide, A.; Gault, F. G. *J. Chim. Phys.* **1974**, *71*, 1329.

(39) Amir-Ebrahimi, V.; Gault, F. G. *Org. Mass. Spectrom.* **1975**, *10*, 711.

(37) Gault, F. G. *Adv. Catal.* **1981**, *30*, 1.

TABLE VII: (A) Aromatization and Hydrocracking and (B) Isomerization of 3-Methylhexane-*methyl*- $^{13}\text{C}$  on Pd/PrO<sub>x</sub> and Pd/ $\gamma$ -Al<sub>2</sub>O<sub>3</sub> ( $T = 360^\circ\text{C}$ ,  $P_{3\text{-MH}} = 5$  Torr;  $P_{\text{H}_2} = 755$  Torr)

A														
support	$\alpha_T$	$\alpha_A$	$a_6(\text{MCH}^+)$				+						+	
PrO <sub>x</sub>	13.7	3.3	0.32	95	3	2			19	14	14			53
PrO <sub>x</sub>	20.2	5.4	0.33	96	2	2			17	18	7			58
Al <sub>2</sub> O <sub>3</sub>	25.3	1.2	0.12	95	5				28	30	1			41
Al <sub>2</sub> O <sub>3</sub> <sup>a</sup>	15.3	3.2	0.28	99				1		18	21	7		54
B														
support	$\alpha_T$	2MH <sup>b</sup>		NH <sup>c</sup>										
		BS, %	CM, %	BS, %	CM, %									
PrO <sub>x</sub>	13.7	44	56	38	62									
Al <sub>2</sub> O <sub>3</sub>	25.3	36	64	26	74									
Al <sub>2</sub> O <sub>3</sub> <sup>a</sup>	15.3	88	12	90	10									

<sup>a</sup>  $P_{\text{H}_2} = 38$  Torr according to ref 12. <sup>b</sup> Pathways calculated according to BS (%) = 2 (50-). <sup>c</sup> Pathways calculated according to BS (%) = 2 ().

TABLE VIII: Syngas Conversion on Pd/REO<sub>x</sub> Catalysts ( $T = 300^\circ\text{C}$ , Total Pressure = 100 atm,  $[\text{H}_2]/[\text{CO}] = 2$ , Catalyst Weight = 500 mg)

support	$\alpha_S^a$	CO <sub>2</sub>	CH <sub>4</sub>	DME	CH <sub>3</sub> OH	C <sub>2</sub> H <sub>5</sub> OH	PropOH	BuOH + PenOH
Al <sub>2</sub> O <sub>3</sub>	7.5	11	11	69	9			
La <sub>2</sub> O <sub>3</sub>	5.8	26	18	14	41			
CeO <sub>2</sub>	20.6	4	3	2	91	traces		
PrO <sub>x</sub>	2.9	11	7		78	2	1	
TbO <sub>x</sub>	3.8	21	14		49	7	5	4

<sup>a</sup> Conversion per gram of catalyst.

is then the 1-6-cyclization on both catalysts (Scheme III). However, the high level of isotopic enrichment of the demethylated fragment ( $a_6 \sim 0.3$ ) on Pd/PrO<sub>x</sub> strongly suggests that fast successive reactions readily occur through 1,5-cyclization and hydrogenolysis (Scheme IV). The occurrence of these successive steps on Pd/PrO<sub>x</sub> is favored by a decrease in hydrogen or an increase in hydrocarbon coverage.

Considering the isomerization pathway, the contribution of self-isomerization, i.e., the rearrangement of the label in the reactant molecule, did not exceed 5% of the initial labeled product on both catalysts (Table VIIA). Within experimental error, the main formation of 2-methylhexane-*methyl*- $^{13}\text{C}$  (Scheme V, e and f) and [1- $^{13}\text{C}$ ]heptanes on both catalysts supports an isomerization mechanism occurring through cyclic adsorbed intermediates instead of a bond shift (Table VIIB), according to the pathways depicted in Scheme V.

We assume that the probability for bond shift isomerization in *n*-heptanes through an ethyl shift (Scheme Va) or a propyl shift (Scheme Vb) are identical, which can be justified by the close analogy in the intermediate species. However, we could not assume that the hydrogenolysis of adsorbed ethylcyclopentane (Scheme Vd) and 1,2-dimethylcyclopentane (Scheme Vc), giving the same isotopic [1- $^{13}\text{C}$ ] *n*-heptane have the same rate, as it has been previously shown that the rate of ethylcyclopentane hydrogenolysis is much higher than that of the 1,2-dimethylcyclopentane hydrogenolysis.<sup>12</sup> Thus we could only determine an overall contribution to the cyclic mechanism pathway. The cyclic mechanism isomerization represented about 55-75% of the overall process in both cases. The important feature is that, as far as isomerization is concerned, Pd/PrO<sub>x</sub> behaved like Pd/ $\gamma$ -Al<sub>2</sub>O<sub>3</sub> catalysts operating under the same conditions of hydrogen pressure.

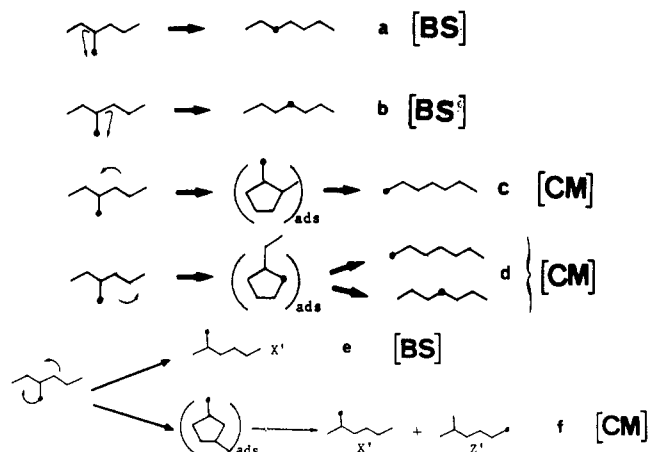
As for isomerization, the hydrocracking process was very similar on both catalysts, the labeled distribution in MCP and the main product of hydrogenolysis being not affected by changing the support (Table VIIA).

3. CO Conversion. The activity and products distribution in CO + H<sub>2</sub> conversion are reported in Table VIII.

The highest activity was shown by the Pd/CeO<sub>2</sub> catalyst. Other catalysts gave rather comparable activity levels.

On La<sub>2</sub>O<sub>3</sub> and CeO<sub>2</sub>, the main product was methanol, whereas on Al<sub>2</sub>O<sub>3</sub> the main product was dimethyl ether (DME). These

SCHEME V



results are in good agreement with reported literature data on palladium catalysts.<sup>5a,c,40</sup> On PrO<sub>x</sub> and TbO<sub>x</sub>, methanol was the main product, but the new feature was the formation of higher alcohols. This was especially the case for TbO<sub>x</sub> support, where C<sub>2</sub>-C<sub>5</sub> alcohols were detected. The C<sub>2</sub>-C<sub>5</sub> alcohol distribution clearly obeys an Anderson-Schulz-Flory law (Figure 8). We observe nevertheless a strong deviation from this law for methanol formation both on TbO<sub>x</sub>- and PrO<sub>x</sub>-supported catalysts.

**Discussion.** The results presented above suggest two questions: (1) What difference can we find in the adsorption and catalytic behaviors between the RE<sub>2</sub>O<sub>3</sub> and REO<sub>2-x</sub> supports? (2) What is the exact nature of the catalytic sites on these supports for both hydrocarbon conversion and syngas reaction? To progress on these two questions, we must clarify first the nature of the support (texture, phase, impurities, etc.) and the metallic dispersion on these supports.

**Nature of the Support.** XRD, TEM, XPS, and volumetric analyses provide us with some useful information on the catalysts

(40) Ryndin, Yu. A.; Hicks, F. F.; Bell, A. T.; Yermakov, Yu. I. *J. Catal.* 1981, 70, 281.

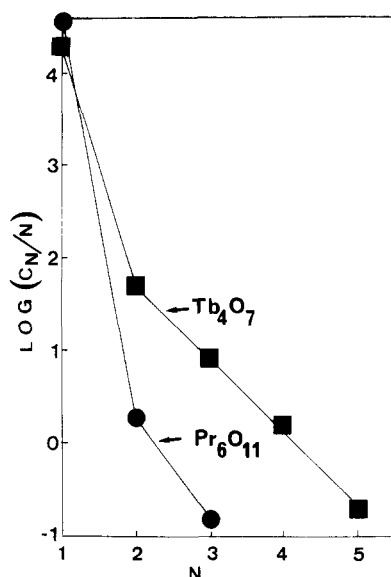


Figure 8. Anderson-Schulz-Flory plot  $\log(C_N/N) = f(N)$  of the alcohols  $C_1$ - $C_5$  distribution on Pd/PrO<sub>x</sub> (●) and Pd/TbO<sub>x</sub> (■).

formed by a transition metal deposited on rare earth oxides.

The first clear information is the exact nature of the support. Both XRD and TEM examinations support the idea of badly crystallized rare earth systems due to easy hydroxide and carbonate species formation.<sup>41</sup> The calcination treatment at 400 °C cannot fully restore the oxide form. Moreover, fluorite oxides exhibit in the range of oxygen stoichiometry  $2 < x < 1.5$  a very rich phase diagram with a large ability to form nonstoichiometric compounds.<sup>42</sup> From XRD and TEM examinations, it is clear that the stable oxide phases of the support are CeO<sub>2</sub>, Pr<sub>6</sub>O<sub>11</sub>, and Tb<sub>4</sub>O<sub>7</sub>, respectively, which means that, for the last two supports, anion vacancies with an ordered periodicity do exist intrinsically. This is an important point on which we shall come back later when discussing the nature of the catalytic active sites.

However, XPS and volumetric experiments can give us additional information on the modification of these oxides under reducing conditions. TPR clearly indicates that hydrogen diffusion on the support occurs during the reduction, whatever the nature of the rare earth oxide. Moreover, the O 1s line shows a high amount of hydroxylated or carbonated oxygen on the surface. RE 3d lines obviously show that La, Pr, and Tb oxides are not further modified upon reduction. On the contrary, CeO<sub>2</sub> is partly reduced, probably to some nonstoichiometric phase CeO<sub>2-x</sub>. This reduction occurs through an extrinsic formation of oxygen vacancies,<sup>43</sup> induced by the presence of both the transition metal and hydrogen. The creation of these vacancies increases the rate of anion diffusion, both by an entropic (number of vacancies) and enthalpic (activation energy) terms and thus can explain the enhanced oxygen diffusion on ceria during the TPO process.<sup>44</sup>

To summarize, we can state that the rare earth oxides investigated in this study as supports of catalysts can be classified into three distinct series: unreducible supports (La<sub>2</sub>O<sub>3</sub>, Nd<sub>2</sub>O<sub>3</sub>) where oxygen vacancies are unlikely to occur whatever the treatment; supports with intrinsic oxygen vacancies (Pr<sub>6</sub>O<sub>11</sub>, Tb<sub>4</sub>O<sub>7</sub>); and support with an extrinsic formation of oxygen vacancies upon reduction (CeO<sub>2-x</sub>).

Another important point which needs to be clarified is the nature and the localization of chlorine on these supports. Chlorine comes from the precursor salt of the transition metal. Elemental analysis gives a high chlorine loading and in some cases (La<sub>2</sub>O<sub>3</sub>, Nd<sub>2</sub>O<sub>3</sub>,

and TbO<sub>3</sub>) the molar ratio Cl/Pd remains close to 2. This indicates that no chlorine evolution occurs during the pretreatment of the catalyst. On the contrary, the chlorine evolution is almost complete on Al<sub>2</sub>O<sub>3</sub>, TiO<sub>2</sub>, ThO<sub>2</sub>, and CeO<sub>2</sub> supports. XRD points out the occurrence of a REOCl phase on most rare earth oxides except CeO<sub>2</sub>. Such a phase is known to be stable under calcination conditions up to high temperatures. It has been shown that only the oxychloride CeOCl is decomposed to CeO<sub>2</sub><sup>45</sup> around 300 °C. Indeed the chlorine surface content, as measured by XPS, decreases during the calcination treatment on PrO<sub>x</sub> and CeO<sub>2</sub>, probably indicating a decomposition which is partial for PrOCl and complete for CeOCl. An oxychloride phase has been evidenced on Pd-Ce and Pd-La/Al<sub>2</sub>O<sub>3</sub> catalysts for large enough rare earth loadings<sup>16a</sup> and has been noticed on Pd/La<sub>2</sub>O<sub>3</sub> catalysts.<sup>46</sup> However, we note on the other hand that the XPS Pd 3d lines give always a weak contribution at high binding energy. The shift of about 3 eV relative to the metallic line could be assigned to a Pd-Cl species formed at the interface of the metal particle and the support, the chlorine species being provided by the oxychloride phase surrounding the metallic particle. The same effect has been observed to a larger extent by XPS and EXAFS on Pd-La and Pd-Ce/Al<sub>2</sub>O<sub>3</sub> catalysts.<sup>51</sup> Upon air admission, part of the chlorine of this phase combined with palladium at the interface of the support, playing the role of a bridge between the transition metal and the support. Under reductive environment, the Pd-Cl bond is broken. On ceria support, the occurrence of such an interaction depends on the calcination temperature due to the instability of the oxychloride phase. On the contrary, on Pd/Al<sub>2</sub>O<sub>3</sub> and Pd/TiO<sub>2</sub>, most chlorine is evolved by the calcination.

In conclusion, we must emphasize here the ability of rare earth oxides to attract the chlorine coming from the precursor salt of palladium. The result is the formation of a stable oxychloride phase surrounding the metallic particle.

**Dispersion of the Metallic Phase.** The metallic dispersion is lower on rare earth oxides than on alumina, except probably for the Pd/CeO<sub>2</sub> catalyst. This is ascertained by TEM visualization, chemisorption measurements, XPS estimation of the metal/support ratio and catalytic activity for MCP conversion.

The absence of chemisorption after a high-temperature reduction is probably not indicative of the real dispersion but of the occurrence of a strong interaction between the metal and the support. This has been described as a nesting of the palladium particle throughout the reduced ceria lattice,<sup>48</sup> encapsulation of the particle by the reduced support,<sup>53</sup> direct electronic interaction,<sup>54</sup> or even alloy formation.<sup>3,34</sup> The calcination treatment restores the hydrogen chemisorption ability on the ceria support. However, chemisorption results are probably not completely reliable both for CO and H<sub>2</sub> chemisorption as CO chemisorbs and could be decomposed even on the support alone as reported by Mitchell et al.<sup>7a</sup> and H<sub>2</sub> spillover onto the support probably occurs even at room temperature. Thus we think that the activity for MCP conversion is more reliable to obtain information on the dispersion state of the transition metal, provided that (i) the metal is fully reduced and (ii) the catalytic activity takes place on the metallic phase at a rate independent of the dispersion. On the first point, the metallic character of palladium, even at low-temperature reduction (150 °C), is checked by XPS. On alumina, however, the MCP conversion is higher after a high-temperature reduction, which suggests that full reduction on alumina requires a reduction up to 400 °C. In the same way Barrault<sup>49</sup> and Turlier<sup>50</sup> report the easy reduction of Ni on such a support. The second point will be discussed later, but we can retain that the MCP reactivity

(45) Klevtsov, O. *Compt. Rend. Acad. Sci.* **1968**, *266*, 385.

(46) Fleisch, T. H.; Hicks, R.; Bell, A. T. *J. Catal.* **1984**, *87*, 398.

(47) Le Normand, F.; Barrault, J.; Kili, K.; Hilaire, L. To be published.

(48) Sanchez, M. G.; Gasquez, J. L. *J. Catal.* **1987**, *104*, 120.

(49) Barrault, J.; Allouche, A.; Paul-Boncour, V.; Hilaire, L.; Percheron, A. *Appl. Catal.* **1989**, *46*, 269.

(50) Turlier, P.; Praliaud, H.; Moral, P.; Martin, G. A.; Dalmon, J. A. *Appl. Catal.* **1985**, *19*, 287.

(51) (a) Le Normand, F.; Garin, F.; Hilaire, L.; Kili, K. Submitted for publication in *J. Chim. Phys.*

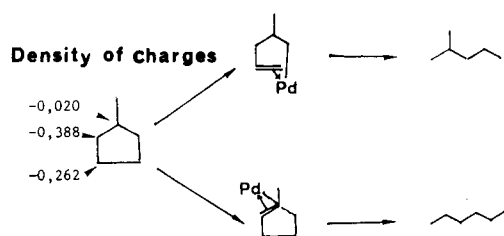
(41) Bernal, S.; Botana, F. J.; Garcia, R.; Rodriguez-Izquierdo, J. M. *React. Solids* **1987**, *4*, 23.

(42) Gschneidner, Jr. K.; Eyring, L. *Handbook of Rare Earths*; North Holland: Amsterdam, 1979; Vol. 3, p 337.

(43) Sorensen, O. T. *Nonstoichiometric Oxides*; Academic Press: New York, 1981; p 12.

(44) Catlow, C. R. *Nonstoichiometric Oxides*, Academic Press: New York, 1981; p 62.

## SCHEME VI



occurs on the metallic particle, even if some interaction with the support may slightly deviate the selectivity. Finally the turnover frequency in MCP conversion has been found independent of the metallic dispersion on Pd/Al<sub>2</sub>O<sub>3</sub>.<sup>51,52</sup> The activity according to the support ranges in the following decreasing order:



The activity for Pd/Al<sub>2</sub>O<sub>3</sub> catalyst is taken after a reduction at 400 °C. This classification is rather in agreement with the observations of the dispersion obtained from TEM or XPS, with particle size ranging from ca. 6 nm on Al<sub>2</sub>O<sub>3</sub> to more than 10 nm on the RE oxides.

In addition, the evolution of the activity with increasing reduction temperature can give us additional information on the nature of the metal-support interaction. We report that the decrease in activity is somewhat higher on rare earth oxides than on titania. The process of strong metal-support interaction has been well studied on this last support and most explanations assume an encapsulation of the metallic particle by some reduced species of the support.<sup>53</sup> This suggests that the mechanism of interaction between the transition metal and the support is at least partly different on TiO<sub>2</sub> and CeO<sub>2</sub>. Sanchez and Gasquez,<sup>48</sup> in the framework of a purely geometric model, have pointed out that reduced fluorite oxides could not bury metallic atoms, a different behavior from the oxides of the cassiterite type such as TiO<sub>2</sub>. However, this model could not explain the strong decrease in catalytic activity occurring with increasing reduction temperature on fluorite oxides. Thus a direct electronic interaction or an alloy formation is also possible.

**MCP Hydrogenolysis.** As reported elsewhere,<sup>52</sup> the activity and selectivity of Pd/Al<sub>2</sub>O<sub>3</sub> in MCP hydrogenolysis is not structure-sensitive when particle sizes are higher than about 3 nm. Here we obtain a small but definite change of selectivity toward 2MP formation on fluorite oxides supports (CeO<sub>2</sub>, PrO<sub>x</sub>, TbO<sub>x</sub>, ThO<sub>2</sub>). The same effect has been pointed out on Pd-Ce/γ-Al<sub>2</sub>O<sub>3</sub> catalysts with increasing Ce content.<sup>47</sup> On the fluorite supports, the activation energies are higher by about 10 kcal/mol relative to Pd/Al<sub>2</sub>O<sub>3</sub>. Moreover, the activation energies fit a unique compensation curve on these supports (and Nd<sub>2</sub>O<sub>3</sub>) which is slightly different on Pd/Al<sub>2</sub>O<sub>3</sub>. To explain this compensation effect, Conner Jr.<sup>36</sup> points out that an increase in the enthalpy of formation (thus in the activation energy) is compensated by an increase of the entropy (thus in the frequency factor) of the metal-adsorbate system. As pointed out elsewhere,<sup>51</sup> the selectivity in MCP hydrogenolysis is governed by the adsorption of MCP on metal giving a σ-alkyl carbon-metal bond. The electronic density of charges calculated by Hoffmann<sup>55</sup> on each carbon atom of the MCP molecule states a high electronic density of charges on the carbon atoms located in α and β of the tertiary carbon (Scheme VI). Thus, taking into account the electrodonor character of the Pd-C bond<sup>56</sup> we can explain that (i) an electronic transfer from the support to the metallic particle increases the 2-MP and NH selectivities and (ii) the activation energy increases. According to this interpretation, the NH selectivity must also

increase. This is not observed, probably due to some steric hindrance. In agreement with that interpretation, the 3d XPS binding energy of palladium is lower by 0.4 eV on the calcined Pd/CeO<sub>2</sub> as compared to Pd/Al<sub>2</sub>O<sub>3</sub>. However, our results can also be explained by morphological changes of the metallic particles<sup>58</sup> (new exposed faces of specific selectivity) induced by the support or by specific reaction rates at the metal-support interface or even on the support. Although blank experiments are negative, we could not exclude some contribution of the support as CeO<sub>2</sub> support is reduced in the presence of palladium as shown by XPS and thus could behave differently from the support alone which is unreduced. However, we could exclude the involvement of basic sites on fluorite oxides, as these oxides have weaker basic sites than RE<sub>2</sub>O<sub>3</sub> oxides<sup>57</sup> whose behavior as support in MCP hydrogenolysis is quite similar to Al<sub>2</sub>O<sub>3</sub>. On the other hand a bifunctional mechanism with the participation of acidic sites is improbable, as carbenium ions intermediates give mainly NH.<sup>60</sup> In the case of specific reaction at the metal-support interface, NH formation is also reported.<sup>59</sup>

In conclusion, the small selectivity change in MCP hydrogenolysis on Pd/fluorite catalyst can be best explained by an electronic interaction with the support, i.e., a modification of palladium density of states induced by the oxide.

**3-MH Aromatization.** Let us summarize briefly the main results of this study on 3-MH reactivity:

Ceria support is not inactive at 360 °C; the main products are hydrocracking and dehydrogenation (including aromatization).

The aromatization activity is higher for Pd/Al<sub>2</sub>O<sub>3</sub> and Pd deposited on fluorite type oxides (CeO<sub>2</sub>, PrO<sub>x</sub>, TbO<sub>x</sub>).

The aromatization selectivity is highest on the PrO<sub>x</sub> and TbO<sub>x</sub> supports.

The selectivity enhancement in aromatization on catalysts supported on fluorite type oxides is due to an increase in the number of active sites.

The high amount of indirect aromatization occurring through 1-5 dehydrocyclization can be related to a change of the hydrogen to hydrocarbon coverage ratio.

Contrarily to aromatization, isomerization occurs mainly through a cyclic mechanism on Pd/Al<sub>2</sub>O<sub>3</sub> and Pd/PrO<sub>x</sub>.

Obviously the large increase in frequency factor on Pd/PrO<sub>x</sub> catalyst can only be taken into account by the creation of new active sites at the interface or even on the support since the palladium dispersion remains lower on these catalysts. Here we must emphasize the role of chlorine present on the support surrounding the metallic particle. Chlorine is well-known as a promoter of reforming on Pt/Al<sub>2</sub>O<sub>3</sub> catalysts, including aromatization. On such a catalyst, the mechanism is bifunctional, chlorine increasing the acidity strength of support sites involved in aromatization.<sup>60</sup> Thus the selectivity in aromatization is generally higher on RE oxides than on Al<sub>2</sub>O<sub>3</sub> or on TiO<sub>2</sub>. However, the increase in chlorine content and the creation of new active sites on the support cannot explain the different behavior between the RE<sub>2</sub>O<sub>3</sub> and the REO<sub>2-x</sub> supports. We must also invoke the stabilization of C<sub>6</sub> and C<sub>5</sub> ring intermediate species on oxygen vacancies of the support due to the generation of strong Lewis acid sites. The C<sub>5</sub> ring species are well-known as byproducts responsible for deactivation in reforming reaction. They can thus provide intermediates for aromatization products, as ascertained here by the high selectivity toward 1-5-cyclic intermediates in the aromatization process. We can invoke also the poor hydrogenation ability of fluorite oxides compared to the other RE<sub>2</sub>O<sub>3</sub>.<sup>8</sup>

(57) Levitskii, I. I.; Minachev, K. M.; Boganov, A. M. *Izv. Akad. Nauk., Ser. Chim.* **1973**, *4*, 762.

(58) Maire, G. L. C.; Garin, F. G. In *Catalysis: Science and Technology*; Anderson, J. R., Boudart, M., Eds.; Springer: Berlin, 1981, p 162.

(59) Kramer, R.; Zuegg, H. *Proceedings of the VIIIth International Congress on Catalysis*; Verlag Chemie: Berlin, 1984; p 275.

(60) (a) Brouwer, D. M. *Prog. Phys. Org. Chem.* **1972**, *9*, 179. (b) Pines, H. *The Chemistry of Catalytic Hydrocarbon Conversion*; Academic Press: New York, 1985; p 61.

(61) (a) Roper, M.; Strutz, H.; Keim, W. *J. Organomet. Chem.* **1981**, *15*, 216. (b) Bowker, M.; Houghton, H.; Waugh, K. C. *J. Chem. Soc., Faraday Trans. 1* **1981**, *77*, 3023.

(52) Del Angel, G. A.; Coq, B.; Ferrat, G.; Figuras, F. *Surf. Sci.* **1985**, *156*, 943.

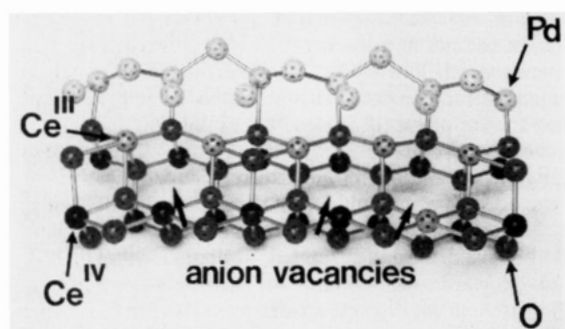
(53) Baker, R. T. K.; Prestidge, E. B.; McVicker, G. B. *J. Catal.* **1984**, *89*, 422.

(54) Horsley, J. A. *J. Am. Chem. Soc.* **1979**, *101*, 2870.

(55) Hoffmann, R. *J. Chem. Phys.* **1963**, *39*, 1399.

(56) Low, J. L.; Goddard, III W. A. *Organometallics* **1986**, *5*, 609.

## SCHEME VII



Isomerization occurs clearly on the metallic site according to a cyclic mechanism which is the main process on palladium. On the contrary an acidic mechanism<sup>60</sup> occurs through a completely different pathway.

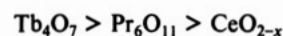
In conclusion, new active sites specific for aromatization are created on Pd deposited on fluorite-type oxide but complementary works are needed to clarify the role of parameters such as chlorine content and oxygen vacancies content on this selectivity.

**Syngas Reactivity.** The important point is the selectivity toward higher alcohols on Pd/PrO<sub>x</sub> and especially Pd/TbO<sub>x</sub> catalysts, since only a few results have been reported for alcohol chain growth on Pd catalysts.<sup>6a,65a</sup> It is generally accepted that the transition metals such as palladium dissociate CO poorly and are weak catalysts for a chain growth of alcohols, whereas Pd deposited on basic rare earth oxides (La<sub>2</sub>O<sub>3</sub>, Nd<sub>2</sub>O<sub>3</sub>) are efficient catalysts for the methanol synthesis.<sup>5</sup> Indeed we find methanol as the main product on all catalysts, except on Pd/Al<sub>2</sub>O<sub>3</sub>.

The chain growth mechanism on noble metals (Rh, Pd) involves a C1 oxygenated insertion into a CH<sub>x</sub> species.<sup>61</sup> We think that dissociation of CO on palladium can occur here as oxygen vacancies exist at the metal-support interface. Burch et al.<sup>62</sup> note on Pd/TiO<sub>2</sub> that the reduction of the support at the metal-support interface helps the adsorption or the dissociation of CO. Dissociation of CO is more probable on Pd/PrO<sub>x</sub> and Pd/TbO<sub>x</sub> where intrinsic vacancies exist in the oxide lattice. On CeO<sub>2</sub> extrinsic vacancies at the metal-support interface can be created by reduction of the support or substitution by an aliovalent cation such as Li<sup>+</sup> in the ceria lattice.<sup>6a</sup> The same authors note, however, that the reduction of the support could also help the CO dissociation by a change in the electronic properties of the metal.<sup>62</sup> Whatever the interpretation, it seems clear that the metal-support interface plays a key role in the dissociation of CO on palladium. Thus we try to depict on Scheme VII the dissociation of CO at the palladium-fluorite oxide interface where the oxygen fills the vacancy and the carbon is partly hydrogenated into a carbene species or another unsaturated hydrocarbon species. The adsorption on adjacent sites of CO together with a carbene species renders possible the CO insertion and thus the chain growth mechanism. Such a mechanism has been already proposed by Van den Berg et al.<sup>63</sup> One important consequence of this mechanism is that C<sub>n-1</sub> hydrocarbons and C<sub>n</sub> alcohols are parallel products obtained through the same intermediate. The parameter that governs the selectivity toward alcohols is the hydrogenation activity of the metal which must decrease to favor the CO insertion step. Many explanations have been put forward in the literature, but the situation remains somewhat unclear today. Some authors have invoked the formation of metallic ions<sup>5c</sup> or on the contrary an electronic enrichment of the metal.<sup>49,62</sup> However, in our case we note that the two supports on which we obtain significant chain growth in syngas conversion (PrO<sub>x</sub>, TbO<sub>x</sub>) are the same on which a high selectivity toward aromatization is observed in 3-MH conversion. As seen before, we explain the high aromatization selectivity by the generation of strong acidic sites on the support

due to the formation of vacancies and to the presence of chlorine. Thus we think that the loss in hydrogenation activity could be explained by the same effects. This implies that the long alcohol chain is stabilized by the support. Returning to Scheme VII, we note that carbene intermediates are likely to occur on palladium. They have been invoked as intermediates in the homologation of hydrocarbons, which occurs specifically on palladium.<sup>64</sup> The formation of a carbene species at the metal-support interface close to an adsorbed and dissociated CO or a formyl species makes possible an insertion mechanism and alcohol formation. Formyl species have been characterized on Rh and Pd/CeO<sub>2</sub> catalysts by IR spectroscopy and chemical trapping.<sup>65</sup>

We note that the high probability of oxygen vacancies at the interface, and consequently the dissociation of CO would favor a large chain growth. According to XRD, the stable forms of the rare earth fluorite oxides are CeO<sub>2</sub>, Pr<sub>6</sub>O<sub>11</sub>, and Tb<sub>4</sub>O<sub>7</sub>, respectively. Pr<sub>6</sub>O<sub>11</sub> and Tb<sub>4</sub>O<sub>7</sub> are incomplete oxides and could be represented by removing 1/3 and 1/2 of the oxygen atoms respectively, along the (111) axis.<sup>42</sup> Thus we could classify the fluorite-type oxides according to the probability of oxygen vacancies as



Thus the probability of periodically distributed oxygen vacancies along the (111) axis is 33 and 50% for Pr<sub>6</sub>O<sub>11</sub> and Tb<sub>4</sub>O<sub>7</sub>, respectively, whereas for CeO<sub>2-x</sub> the probability is unknown but could not be zero as extrinsic vacancies are created by reduction. We compare the probability of oxygen vacancies which are formed along an (111) axis with the probability of chain growth  $\alpha$  deduced from the slope of the Schulz-Flory plot according to

$$\log C_n = \log \frac{1-\alpha}{\alpha} + n \log \alpha \quad (12)$$

We find that these probabilities are 33 and 45% for Pd/Pr<sub>6</sub>O<sub>11</sub> and Pd/Tb<sub>4</sub>O<sub>7</sub>, respectively. The good correlation obtained between the two sets of probabilities clearly suggests a strong correlation between the occurrence of oxygen vacancies at the metal-support interface and the chain growth of alcohols. The absence of significant chain growth on Pd/CeO<sub>2</sub> catalyst, in spite of the reduction of the support as evidenced by XPS, can be due to (i) the lesser extent of extrinsic oxygen vacancies created by the reduction and (ii) more probably to the randomly or disordered distribution of vacancies. However, Diagne et al.<sup>6a</sup> have shown that chain growth can be obtained on ceria supports by adjunction of lithium, this cation increasing probably the oxygen vacancies. Obviously, however, these results need further confirmation on other fluorite-type oxides, as only two nonstoichiometric oxides are involved in this work. Oxygen vacancies may be created intrinsically as stable forms of nonstoichiometric oxides or extrinsically through chemical reduction, substitution by an aliovalent cation, or formation of mixed oxides.

## V. Conclusion

In conclusion, the main points of this work are the following.

1. Rare earth oxides have been classified into three classes according to their ability to create anionic vacancies in the presence of the transition metal: unreducible oxides of the type RE<sub>2</sub>O<sub>3</sub>; fluorite oxides with intrinsic anionic vacancies such as Pr<sub>6</sub>O<sub>11</sub> and Tb<sub>4</sub>O<sub>7</sub>; and fluorite oxides with extrinsic anionic vacancies such as CeO<sub>2-x</sub> created during the reduction process in the presence of the transition metal.
2. Catalytic activity and selectivity toward varied probes exhibit changes that can be best explained by (i) an electronic interaction for the small selectivity change in MCP hydrogenolysis on catalysts supported on fluorite-type oxides; (ii) a bifunctional mechanism for the high aromatization selectivity in 3-MH conversion on catalysts supported on intrinsic fluorite-type oxides; (iii) a

(62) (a) Bracey, J. D.; Burch, R. *J. Catal.* **1984**, *86*, 384. (b) Burch, R.; Flambart, A. R. *J. Catal.* **1982**, *78*, 389.

(63) Van den Berg, F. G. A.; Gletzer, J. H. E.; Sachler, W. M. H. *J. Catal.* **1985**, *93*, 340.

(64) O'Donohoe, C.; Clarke, J. K. A.; Rooney, J. J. *J. Chem. Soc., Faraday Trans. 1* **1980**, *76*, 345.

(65) (a) Favre, T. L. F.; Lee, G. v. d.; Poncet, V. *J. Chem. Soc., Chem. Commun.* **1985**, 230. (b) Kiennemann, A.; Breault, R.; Hindermann, J. P.; Laurin, M. *J. Chem. Soc., Faraday Trans. 1* **1987**, *83*, 2119.

mechanism of chain growth at the interface of the transition metal and of intrinsic fluorite-type oxide for the dissociation of CO on palladium and the formation of high alcohols in syngas conversion.

Some points however remain unclear. Thus a high alcohol selectivity is found on the intrinsic fluorite-type oxide. The catalytic site has been assigned to a set formed by transition-metal atom (or adjacent atoms) and a couple of adjacent vacant anionic sites and anionic sites on the support (Scheme VII). Now we may expect from the intrinsic nature of these oxides an ordered distribution of surface anionic vacancies. Thus the specific nature

of the catalytic site may induce some special alcohol selectivity rather than a Schulz–Flory distribution. To test this hypothesis, further work must be undertaken in order to prepare catalysts supported on fluorite-type oxides with a controlled and homogeneous distribution of anionic vacancies.

**Acknowledgment.** Many thanks are due to Mr. Lavergne (Université de Paris VI), Mrs. Bacri, and Mr. Vennegues (Université de Strasbourg) for TEM, BET, and XRD experiments, respectively.

## Photoionization on Insulator Surfaces. Diffuse Reflectance Laser Flash Photolysis of Distyrylbenzenes Adsorbed on Silica and Alumina

Dieter Oelkrug,\* Steffen Reich,

*Institut für Physikalische und Theoretische Chemie der Universität, D-7400 Tübingen, Federal Republic of Germany*

Francis Wilkinson, and Philip A. Leicester

*Department of Chemistry, University of Technology, Loughborough, Leicestershire, LE11 3TU, United Kingdom (Received: March 28, 1990; In Final Form: July 19, 1990)*

The absorption and fluorescence of *o*-, *m*-, and *p*-distyrylbenzenes on surfaces of polycrystalline silica and alumina were investigated in the adsorbed state. Time-resolved diffuse reflectance transient absorption spectra were recorded following pulsed nanosecond laser excitation at 354 nm. In each case, a long-lived transient was detected and assigned to radical-cation absorption, and in two cases a short-lived transient was observed and assigned to triplet–triplet absorption. The radicals were also detected by ESR spectroscopy after laser excitation. Experimental observations of the laser fluence dependence of the radical-ion formation efficiency are consistent with a mechanism involving the sequential absorption of two photons during the same laser pulse. It is shown that model calculations for one- and two-photon excitation processes give predictions that are in good agreement with the measurements of the triplet-state and radical-ion production, respectively. The radicals decay by electron–ion recombination. The experimentally observed decay curves are well described by a temperature-activated diffusion model. Decay kinetics are discussed and tested in relation to this theoretical treatment.

### Introduction

Adsorbed organic molecules can be photoionized with photon energies far below their ionization potentials, IP, as long as the adsorbent consists of a semiconductor. After photoexcitation of either the adsorbent or the adsorbate, an electron or hole is transferred between the adsorbate and an energy band of the semiconductor, and the excess charge diffuses into the bulk of the semiconductor, leaving the radical ion on the surface. The corresponding process on insulators is very unfavorable since low-energy conduction bands are not available. Nevertheless, radical cations of conjugated hydrocarbons with IP > 7.5 eV can be produced on insulators with laser pulses that have photon energies of only 3–4 eV.<sup>1,2</sup> Beck and Thomas propose that photoionization on insulator surfaces is the result of two-photon absorption and that the adsorbed radical decays via recombination involving either electron tunneling or a diffusion process.<sup>1</sup> The adsorbed radical ions have been detected by the method of diffuse reflectance laser flash photolysis<sup>3,4</sup> using polycrystalline microporous metal oxides such as silica or alumina as adsorbents.

Until now, neither the mechanism of the creation nor the deactivation of the adsorbed radicals was fully understood. One of the aims of this paper is to quantify these reaction steps on the basis of new experimental data. Since a laser pulse produces in a strongly light-scattering sample a very high photon flux density within a very small volume, it is reasonable to assume that nonlinear optical effects are of importance in the excitation process. An obvious starting point is to consider two consecutive absorption

steps. This process is well understood from jet-beam experiments in the gas phase,<sup>5,6</sup> where the radicals are stabilized in molecular donor–acceptor clusters. Similar processes are assumed to operate also in the liquid phase,<sup>7–9</sup> in micelles,<sup>10</sup> and in polymers,<sup>11</sup> and the proof is mainly given by showing that the initial rate of the radical formation increases quadratically with the intensity of the exciting light. It is especially difficult to evaluate corresponding experiments in light-scattering media because the photometric laws are much more complex than in transparent media and because even a very small self-absorption by the adsorbent is crucial for the initial rate of transient formation. However, we have been able to develop numerical methods, based on the Kubelka–Munk model,<sup>12</sup> which allow us to quantify diffuse reflectance laser flash experiments with respect to decay kinetics,

- (1) Beck, G.; Thomas, J. K. *Chem. Phys. Lett.* **1983**, *94*, 553.
- (2) Oelkrug, D.; Krabichler, G.; Honnen, W.; Wilkinson, F.; Willsher, C. *J. Phys. Chem.* **1988**, *92*, 3589.
- (3) Wilkinson, F. *J. Chem. Soc., Faraday Trans. 2* **1986**, *82*, 2073.
- (4) Wilkinson, F.; Willsher, C. *J. Chem. Phys. Lett.* **1984**, *104*, 272.
- (5) Brutschy, B.; Janes, C.; Eggert, J. *Ber. Bunsen-Ges. Phys. Chem.* **1988**, *92*, 74.
- (6) Rühl, E.; Brutschy, B.; Bisling, P.; Baumgärtel, H. *Ber. Bunsen-Ges. Phys. Chem.* **1988**, *92*, 194.
- (7) Grätzel, M.; Thomas, J. K. *J. Phys. Chem.* **1974**, *78*, 2248.
- (8) Thomas, J. K.; Piccolo, P. *Adv. Chem. Ser.* **1980**, *184*, 97.
- (9) Bauer, H.; Reske, G. *J. Photochem.* **1978**, *9*, 43.
- (10) Almgren, M.; Thomas, J. K. *Photochem. Photobiol.* **1980**, *31*, 329.
- (11) Tsuchida, A.; Nakano, M.; Yoshida, M.; Yamamoto, M.; Wada, Y. *Polym. Bull. (Berlin)* **1988**, *20*, 297.
- (12) Kubelka, P. *J. Opt. Soc. Am.* **1948**, *38*, 448.

\* To whom correspondence should be addressed.